

AD-A064 755

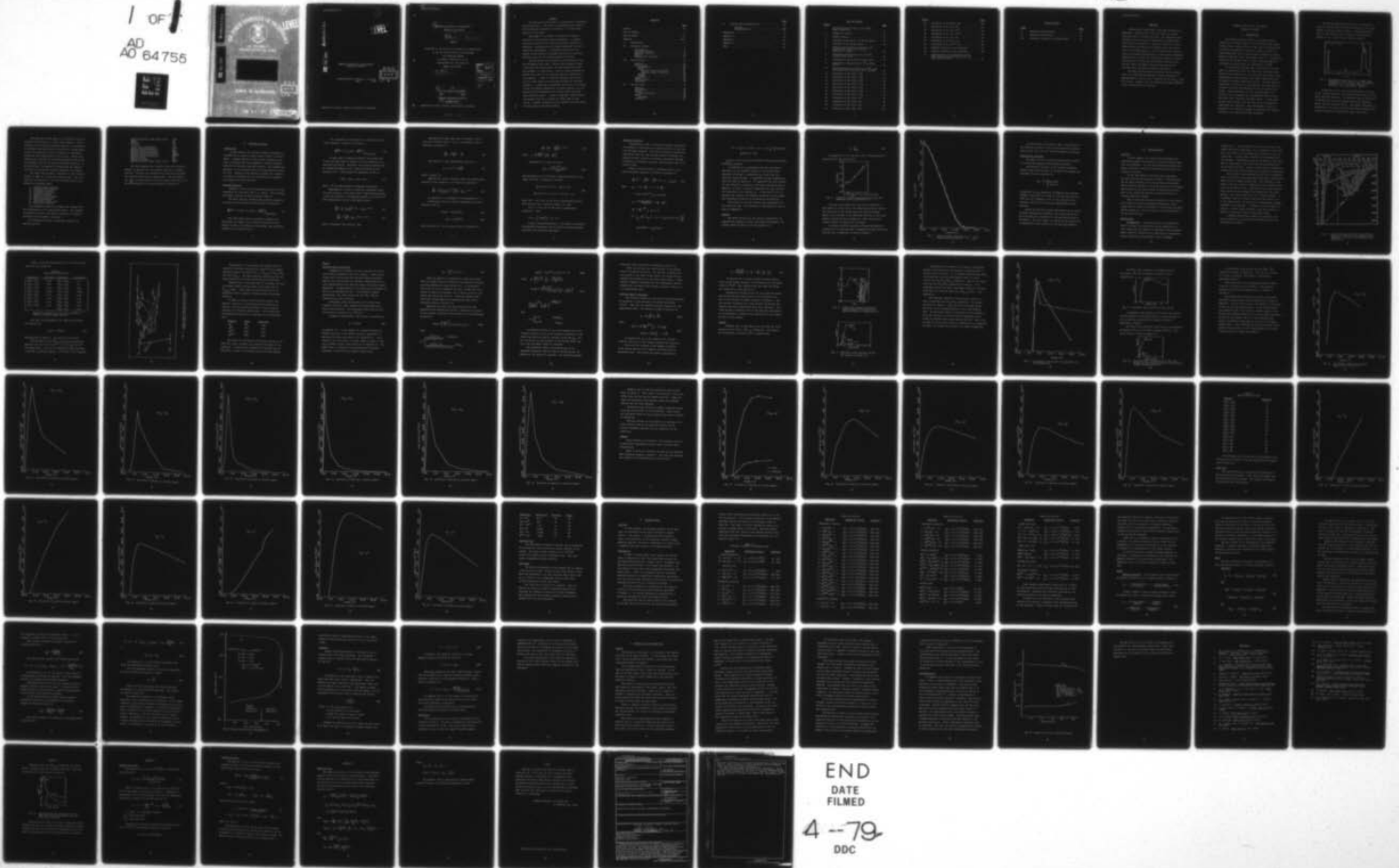
AIR FORCE INST OF TECH WRIGHT-PATTERSON AFB OHIO SCH--ETC F/G 20/5
TEMPORAL EVOLUTION OF THE MERCURY-CHLORIDE DISCHARGE. (U)

UNCLASSIFIED

DEC 78 W R ERCOLINE
AFIT/GEP/PH/78D-2

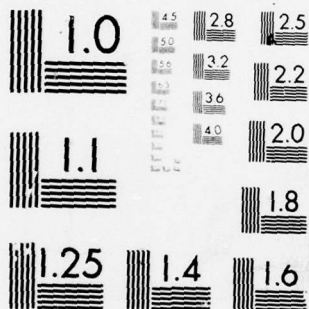
NL

1 OF 1
AD
AO 64756



END
DATE
FILMED

4--79
DDC



MICROCOPY RESOLUTION TEST CHART
 NATIONAL BUREAU OF STANDARDS-1963-A

ADA 064755

DDC FILE COPY

AIR FORCE INSTITUTE OF TECHNOLOGY LEVEL 4



AIR UNIVERSITY
UNITED STATES AIR FORCE



SCHOOL OF ENGINEERING

WRIGHT-PATTERSON AIR FORCE BASE, OHIO

DDC
RECEIVED
FEB 22 1979
A

79 01 30

DISTRIBUTION STATEMENT
Approved for public release
Distribution Unlimited

①

ADA064755

LEVEL #

DDC FILE COPY

TEMPORAL EVOLUTION OF THE MERCURY-
CHLORIDE DISCHARGE

DDC
RECEIVED
FEB 22 1979
A

AFIT/GEP/PH/78D-2 William R. Ercoline
Capt USAF

Approved for public release; distribution unlimited.

79 01 30 168

6
TEMPORAL EVOLUTION OF THE MERCURY-
CHLORIDE DISCHARGE.

9 Master's Thesis

THESIS

Presented to the Faculty of the School of Engineering
of the Air Force Institute of Technology
Air Training Command
in Partial Fulfillment of the
Requirements for the Degree of
Master of Science

12 90 P.

SEARCHED	INDEXED
SERIALIZED	FILED
DEC 1978	
AFIT	
A	

10 by
William R. Ercoline ~~B.S.~~

Capt USAF

Graduate Engineering Physics

11 December 1978

Approved for public release; distribution unlimited.

012 225

ell

Preface

The mercury-chloride laser is a potentially outstanding high energy laser. The need for understanding the significant microscopic processes is essential if a large scale system is to be built.

This paper is an attempt to develop the temporal evolution of the mercury-chloride discharge. A complete numerical solution of the electron Boltzmann equation is developed. Cross-sections for higher metastable levels of mercury are determined. A numerical solution for the change of each species is incorporated with the numerical Boltzmann code for the overall temporal evolution.

Several people have provided me with assistance and aid throughout this study. Without the exchange of ideas I have had with these people, this paper would lack some key elements. In particular, I want to thank Ed Seward of my GEP 78-D class for the numerous hours of assistance on the computer. I want to thank Hal Hastings and Tom Gist for the joint effort in numerically solving the Boltzmann equation. A large debt of gratitude is owed to A. M. Hunter of the AFIT Physics Department, my thesis advisor, for the guidance and encouragement when things looked as though they would fall apart. I want to thank Mrs. Sharon Maruna for doing a fine job in typing the final copy of this thesis. Finally, a special note of thanks to my wife Kathy, for her patience and understanding.

Contents

	<u>Page</u>
Preface	ii
List of Figures	v
List of Tables	vii
Abstract	viii
I. Introduction	1
II. Boltzmann Equation	5
Introduction	5
Boltzmann Equation	5
Numerical Solution	9
Results	10
Pumping Rate Constants	13
III. Cross Sections	14
Overview	14
Mercury (Hg)	14
Introduction	14
Theory	20
Electron Impact Excitation	20
Electron Impact Ionization	23
Results	24
Summary	37
Argon (Ar)	43
Chlorine (Cl ₂)	50
Conclusion	50
IV. The HgCl Model	51
Overview	51
Introduction	51
Theory	56
General Reactions	56
Model	57
Intensity	62
Discussion	63

	<u>Page</u>
V. Results and Recommendations	65
Results	65
Recommendations	68
References	71
Appendix A	73
Appendix B	74
Appendix C	76
Vita	78

List of Figures

<u>Figure</u>		<u>Page</u>
1	Microdensitometer trace of B→X HgCl laser transition	2
2	Rockwood's results	11
3	Stamm's results.	12
4	Revelant Energy Levels for the Hg System . . .	16
5	Lifetimes of Hg energy levels	18
6	Elastic-and inelastic-scattering cross sections for electrons in Hg as a function of energy	25
7	Excitation cross-sections for the 6^3P levels, after Kenty	25
8	Calculated cross section from Gryzinski . . .	27
9	Excitation cross-section for 6^1P_1 , after Penney	28
10	Cross sections for excitation of 7^3S_1 from the ground state and 6^3P_0 , after Yavorski . .	28
11	Excitation of Hg, $6^3P_2 - 7^3S_1$	30
12	Excitation of Hg, $6^1S_0 - 6^3D_2$	31
13	Excitation of Hg, $6^3P_2 - 6^3D_2$	32
14	Excitation of Hg, $7^3S_1 - 6^3D_2$	33
15	Excitation of Hg, $6^3P_2 - 6^1P_1$	34
16	Excitation of Hg, $6^1P_1 - 7^3S_1$	35
17	Excitation of Hg, $6^1P_1 - 6^3D_2$	36
18	Ionization of Hg, $6^1S_0 - Hg^+$	38
19	Ionization of Hg, $6^3P_2 - Hg^+$	39
20	Ionization of Hg, $6^1P_1 - Hg^+$	40
21	Ionization of Hg, $7^3S_1 - Hg^+$	41

<u>Figure</u>		<u>Page</u>
22	Ionization of Hg, $6^3D_2 \rightarrow Hg^+$	42
23	Excitation of Ar, $Ar \rightarrow Ar^*$	44
24	Excitation of Ar, $Ar \rightarrow Ar^{**}$	45
25	Excitation of Ar, $Ar^* \rightarrow Ar^{**}$	46
26	Ionization of Ar, $Ar \rightarrow Ar^+$	47
27	Ionization of Ar, $Ar^* \rightarrow Ar^+$	48
28	Ionization of Ar, $Ar^{**} \rightarrow Ar^+$	49
29	Temporal Evolution of KrF discharge	61
30	Temporal Evolution, HgCl discharge	69
31	Cross-sections for transitions of the first and second kind between 6^3P_1 and 6^3P_2 , after Yavorski	73

List of Tables

<u>Table</u>		<u>Page</u>
I	Transition Probabilities	17
II	Mercury Cross Sections	43
III	Processes included in Discharge Model	52

Abstract

Computational simulations of the HgCl discharge are discussed. Equations that model the laser are solved simultaneously as functions of time. The discharge model includes electron losses by dissociative attachment and dissociative recombination. Electron sources are direct electron beam ionization and ionization from the excitation of the atomic species. The excitation and ionization rates are obtained from solutions to the electron Boltzmann equation which includes the following processes: inelastic collisions of the first and second kind, heating by the electric field, secondary electron production by the electron beam, and electron-electron collisions.

The HgCl discharge model determines two conclusions. First, the significant metastable levels of Mercury for determining the reaction rate constants are the $6^3P_{0,1,2}$ and 6^1P_1 levels. Second, that the discharge is highly sensitive to the concentration of chlorine.

TEMPORAL EVOLUTION OF THE MERCURY-
CHLORIDE DISCHARGE

I. Introduction

The mercury-chloride molecule is presently being studied as a possible source for an efficient, high energy, visible laser. Lasing action in HgCl from an electron beam controlled discharge was reported in August of 1977 by a joint Maxwell-SRI team of Tang, Hunter, Oldenettel, Howton, Huestis, Eckstrom, Perry, and McCusker (Ref 1). In addition, Parks (Ref 2) and Eden (Ref 3) report observing lasing in the mercury-chloride laser at a wavelength of $5576\overset{\circ}{\text{A}}$.

As the mercury-chloride laser is developed, the need grows to understand better the microscopic processes which determine the population of the upper and lower laser levels. Understanding these processes will enable experimentalists to design a variable large-scale system. The best method to understand the system is to determine all the important contributing reactions theoretically within an order-of-magnitude. These reactions, or their corresponding cross sections, can be compared with experimental data to determine both their importance and exact value. In this paper, as many reactions and cross sections as can be determined significant are tabulated. This information is then incorporated in a numerical program to determine the temporal evolution of the mercury-chloride discharge.

The mercury-chloride lasing action is obtained by using an electron-beam controlled discharge to pump a gas mixture of mercury-chlorine-argon. A microdensitometer trace of the lasing action is given in the article by Hunter, et al. (Ref 1) and is shown in Figure 1.

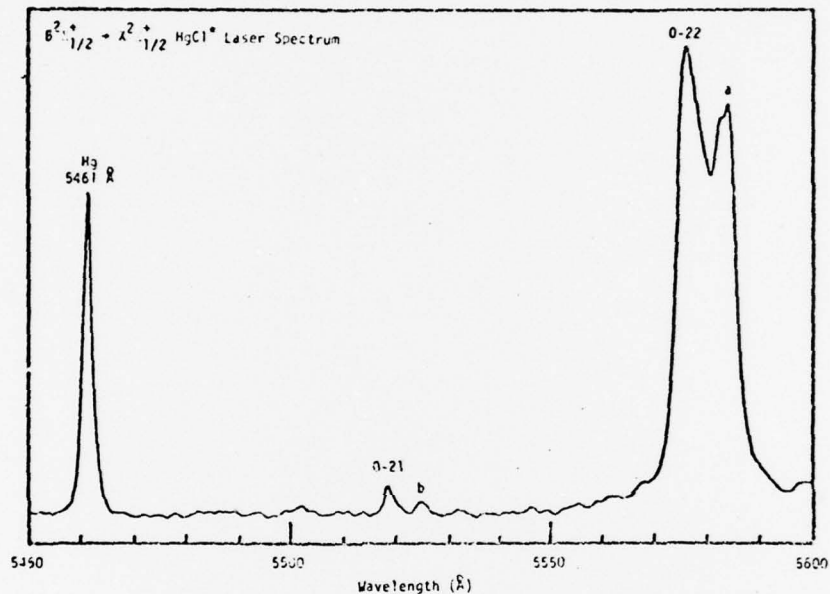


Fig. 1. Microdensitometer trace of B X HgCl laser transition: shown here is also the reference Hg 5461-A° line. Pressure: Hg/Cl₂/Ar - 10/8/1500 torr respectively. (Ref²1).

In addition to the obvious characteristic of lasing in the visible spectrum, the mercury-chloride laser has two other important features. The potential quantum efficiency is 45% and the shorter wavelength means more energy per photon than the infrared lasers. The quantum efficiency is determined by the ratio of the emitted photon energy to the energy necessary for creating the upper laser level.

The approach of this paper is to analyze the mercury-chloride gas evolution in a three step sequence. First, a solution of the electron Boltzmann equation is constructed to determine the distribution of electrons in energy space. Second, the metastable levels of mercury are determined along with their appropriate cross sections. These cross sections are necessary for calculating metastable and ionization pumping rates by the electron Boltzmann equation. In the third step, the physics for determining the temporal evolution of the mercury-chloride discharge is developed.

The third step includes a tabulation of all reactions thought to apply to the mercury-chloride laser. The reactions are an extension of the work of Summers (Ref 4) and include the following types:

1. electron-beam ionization
2. electron loss reactions
3. metastable formation
4. secondary ionization
5. excimer formation
6. excimer loss mechanisms
7. three body reactions
8. Penning ionization
9. lower level excimer loss
10. metastable transfers

Any assumptions made in this paper are included with the establishment of the appropriate theory. The validity of classical mechanics and quantum mechanics is a general assumption made throughout the paper.

The following notation is used when referring to specific species:

Mercury-Chloride (lower laser level)	HgCl
Argon	Ar
Mercury	Hg
Chlorine	Cl ₂
Argon (First Metastable)	Ar*
Argon (Second Metastable)	Ar**
Mercury (First Metastable)	Hg*
Mercury (Second Metastable)	Hg**
Mercury (Third Metastable)	Hg***
Mercury (Fourth Metastable)	Hg****
Argon (ionized)	Ar ⁺
Mercury (ionized)	Hg ⁺
Mercury-Chloride (upper laser level)	HgCl*

The term "pumping rate" refers to the rate at which a species is excited into a metastable level by a secondary electron. Reaction rate constants are those rate constants for reactions other than a pumping rate. Any time derivative, $\frac{dn}{dt}$, is abbreviated by the more common form \dot{n} and n_i is the abbreviation for the number density of species i .

II. Boltzmann Equation

Introduction

In this chapter, the electron energy distribution in a plasma with an applied steady electric field is investigated. A simple analysis to the electron Boltzmann equation is developed and then expanded to include necessary terms for an accurate numerical solution. The complete explanation of the numerical solution is maintained by Hunter (Ref 21). Results of the numerical solution are compared to results of Rockwood (Ref 5) and results by a numerical code supplied by Stamm (Ref 29).

Boltzmann Equation

Analysis of the electron energy distribution is found throughout the literature (Ref 5, 7, and 8). The following development follows the work of Nielsen (Ref 7).

The basic function governing the electron energy distribution is the Boltzmann equation shown in equation 1.

$$\left. \frac{\partial f(\vec{v})}{\partial t} + \vec{v} \cdot \nabla f(\vec{v}) + \vec{a} \cdot \nabla_{\vec{v}} f(\vec{v}) = \frac{\partial f(\vec{v})}{\partial t} \right)_{\text{Collisions}} \quad (1)$$

The first three terms of equation 1 represent respectively the change of the velocity distribution with respect to time, the diffusion of particles, and the motion imparted by an external force.

For a spatially uniform gas with a constant electric field, equation 1 reduces to equation 2.

$$\left. \frac{\partial f(\bar{v})}{\partial t} + \bar{a} \cdot \nabla_{\bar{v}} f(\bar{v}) = \frac{\partial f(\bar{v})}{\partial t} \right) \text{Collisions} \quad (2)$$

In many cases of physical interest, the second term on the left hand side of equation 2 is not expected to impart much net motion. Therefore, the electron distribution is considered symmetric with a small anisotropy in the direction of \bar{v} . This prompts the expansion of $f(\bar{v})$ as

$$f(\bar{v}) = f_0(v) + f_1(v) \cos \theta \quad (3)$$

where θ is the angle between the applied field and \bar{v} .

Expressing \bar{v} in terms of spherical coordinates (with \bar{a} in the direction of the polar axis), substituting equation 3 back into equation 2, multiplying equation 2 by $(\cos \theta)^{0,1}$ then integrating over all solid angles yields

$$\frac{\partial f_0}{\partial t} + \frac{a}{3} \left(\frac{1}{v^2} \frac{\partial v^2}{\partial v} f_1 \right) = \frac{1}{4\pi} \int Q d\Omega \quad (4)$$

$$\frac{\partial f_1}{\partial t} + \frac{a}{3} \frac{\partial f_0}{\partial v} = \frac{3}{4\pi} \int \cos \theta Q d\Omega \quad (5)$$

where Q represents the collision term.

Expressing the right hand side of equation 5 as an effective collision time (τ) for f_1 , the equation can be rewritten as equation 6.

$$\frac{\partial f_1}{\partial t} + \frac{a}{v} \frac{\partial f_0}{\partial v} = - \frac{f_1}{\tau} \quad (6)$$

The solution to this differential equation is

$$f_1 = A e^{-vt} - \frac{a}{v} \frac{\partial f_0}{\partial v} \quad (7)$$

where v equals $1/\tau$.

Ignoring the initial transient time, and substituting equation 7 into equation 4, the result is equation 8.

$$\frac{\partial f_0}{\partial t} - \frac{a^2}{v} \frac{1}{v^2} \frac{\partial}{\partial v} \left[v^2 \frac{\partial f_0}{\partial v} \right] = \frac{1}{4\pi} \int Q d\Omega \quad (8)$$

In equation 8, v is assumed to be independent of v .

Converting to the more useful energy space, by way of equation 9 and 10,

$$f(\epsilon)d\epsilon = 4\pi f_0(v)v^2 dv, \quad (9)$$

$$v(\epsilon) = (2\epsilon/m)^{1/2}, \quad (10)$$

and recalling $a m = eE$, the final result is equation 11.

$$\frac{\partial f}{\partial t} + \frac{\partial J}{\partial \epsilon} = \frac{2\epsilon^{1/2}}{m^{3/2}} \int Q d\Omega \quad (11)$$

where $J = \frac{2}{3} \frac{e^2 E^2 \epsilon}{mv} \left[\frac{f}{2\epsilon} - \frac{\partial f}{\partial \epsilon} \right]$

Relating $f(\epsilon)$ to $f_0(\epsilon)$ by way of

$$f(\epsilon) = \frac{4\pi \sqrt{2} \epsilon^{1/2} f_0(\epsilon)}{m^{3/2}} \quad (12)$$

and expressing Q as an inelastic collisional process, the right hand side of equation 11 becomes

$$\begin{aligned} & n_{\beta}^* f(\epsilon - \Delta\epsilon) R'(\epsilon - \Delta\epsilon) - n_{\beta} f(\epsilon) R(\epsilon) \\ & - n_{\beta}^* f(\epsilon) R'(\epsilon) + n_{\beta} f(\epsilon + \Delta\epsilon) R(\epsilon + \Delta\epsilon) \end{aligned} \quad (13)$$

where $R(\epsilon) = \sigma(\epsilon) v(\epsilon)$ is the rate of producing electrons with velocity $v(\epsilon)$, losing an energy $\Delta\epsilon$, and

$R'(\epsilon) = \sigma'(\epsilon) v(\epsilon)$ is the rate of superelastic collisions. Also,

$$\sigma'(\epsilon) = \left[\frac{\epsilon + \Delta\epsilon}{\epsilon} \right] \sigma(\epsilon + \Delta\epsilon)$$

by way of microreversibility. The result is identical to Rockwood's derivation (Ref 5) without electron-electron collisions and ionization processes.

Numerical Solution

Determining as many collisional processes as possible is necessary in developing an accurate solution to the electron Boltzmann equation. The entire solution is maintained with Hunter (Ref 21), and includes elastic collisions (including electron-electron), inelastic collisions, heating, ionization by secondary electrons, and ionization due to an electron beam.

Using a notation similar to Rockwood (Ref 5), the entire Boltzmann equation is written in equation 14.

$$\frac{\partial n}{\partial t}(\epsilon) = -\frac{\partial J_{ee}}{\partial \epsilon} - \frac{\partial J_f}{\partial \epsilon} + R^* + R^+ + \sum_s S_s(\epsilon) \quad (14)$$

where $J_{ee} = \bar{v} \left[n \left(\frac{KT}{2} - \epsilon \right) - KT\epsilon \frac{\partial n}{\partial \epsilon} \right]$

$$\bar{v} = 2mN (2\epsilon/m)^{1/2} \sum_s q_s \sigma_s(\epsilon) / M_s$$

$$J_f = \frac{2 N e^2 (E/N)^2 \epsilon}{3m (v/N)} \left[\frac{n}{2\epsilon} - \frac{\partial n}{\partial \epsilon} \right]$$

$$\frac{v}{N} = \left(\frac{2\epsilon}{m} \right)^{1/2} \sum_s q_s \sigma_s(\epsilon)$$

$$R^* = \sum_{s,j} N_s^0 \left[R_{sj}(\epsilon + \Delta\epsilon) + R'_{sj}(\epsilon - \Delta\epsilon) n(\epsilon - \Delta\epsilon) \frac{N_s^j}{N_s^0} \right]$$

$$-R_{sj}(\epsilon)N(\epsilon) - R_{sj}(\epsilon)N(\epsilon)]$$

$$R^+ = [R_S^i (\epsilon + \Delta\epsilon)n(\epsilon + \Delta\epsilon) + \delta(\epsilon) \int_{\Delta\epsilon}^{\infty} R_S^i(\epsilon)n(\epsilon)d\epsilon - R_S^i(\epsilon)n(\epsilon)] N_S^0$$

$\sum_S S_S(\epsilon)$ = rate at which an external electron beam creates secondary electrons.

In equation 14, q_S represents the mole fraction of species s , σ_S the momentum transfer cross section from electrons of energy ϵ to molecules N_S , e and m are the electron charge and mass. T represents the gas temperature, and M the mass of species s . R^* represents the rate constant for all inelastic collisions of the first and second kind of species s to level j , while R^+ represents the rate constant for ionization of all species N_S . In the term R^+ , $\delta(\epsilon)$ represents the creation of secondary electrons at zero energy. This assumption allows for a conservation of particles.

The results of the next section were determined with the numerical code. The technique of developing the code is shown in Appendix C.

Results

The drift velocity for the electron distribution is computed and compared to those calculated by Rockwood. The results shown in Figure 2 are from equation 15.

$$V_d = \frac{\dot{\epsilon}}{En_e q} \quad (15)$$

In equation 15, $\dot{\epsilon}$ is the time rate of energy gained by electrons from the dc field (E).

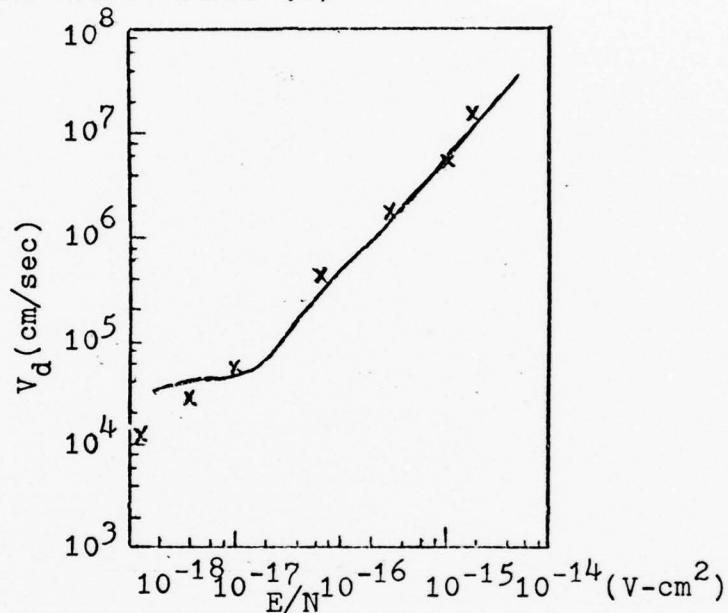


Fig. 2. Rockwood's results represented by solid line. Numerical result represented by X.

The bend at the lower E/N value is not found due to the coarse bin width used in the numerical solution, and the fact that most of the energy goes into elastic heating which is not included in the numerical solution at this time. Elastic collisions were included at a later time and the results matched throughout the E/N range.

A similar numerical generated electron distribution function for an Argon pure gas is supplied by Stamm and Bailey (Ref 29) and a comparison is shown in Figure 3.

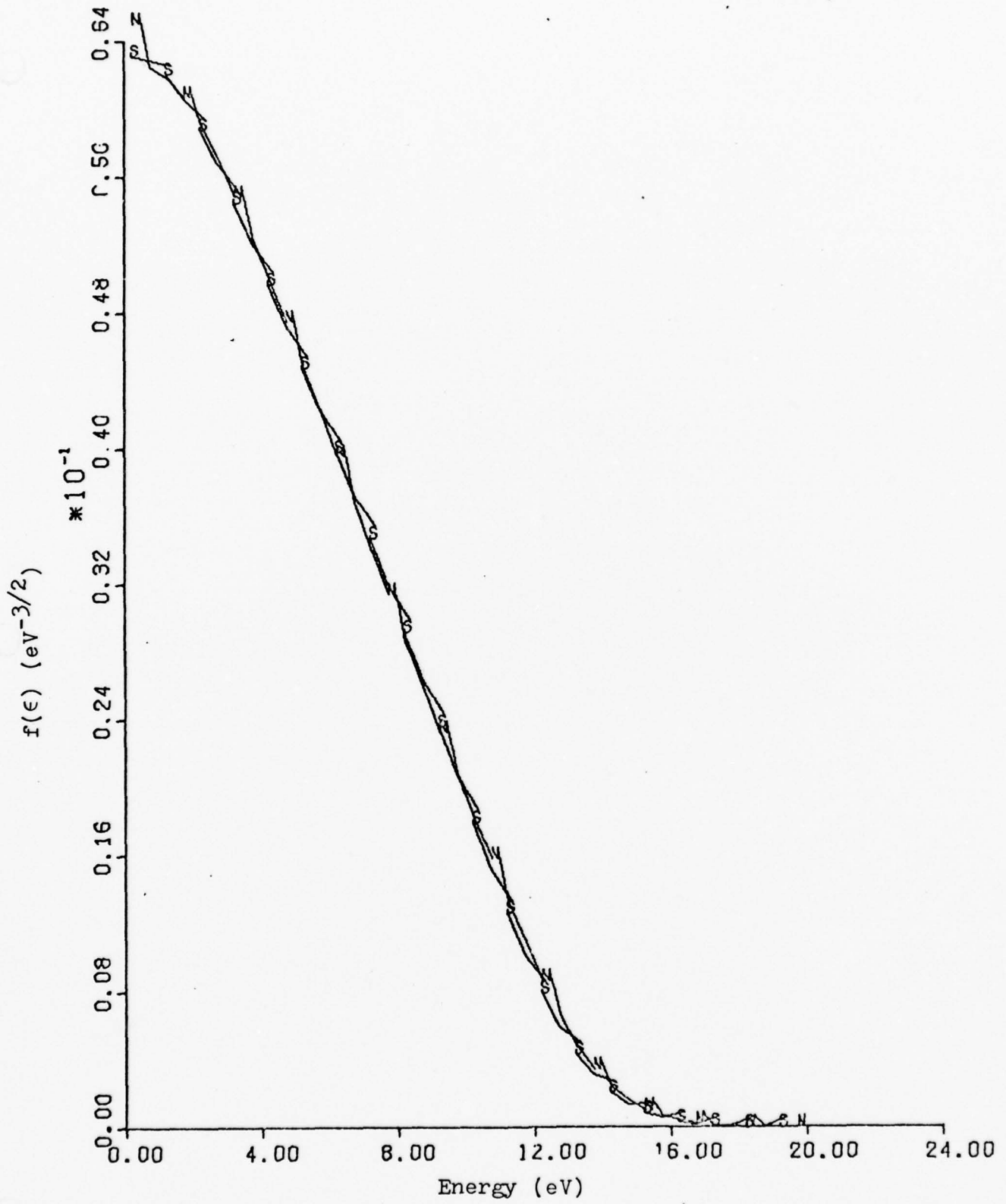


Fig. 3. Stamm's results indicated by S line.
Code results indicated by N line.

As can be seen from Figures 2 and 3, the results of the numerical solution to the electron Boltzmann equation agree rather well with the other two numerical solutions.

Pumping Rate Constants

The major use of the electron distribution function is to calculate pumping rates and drift velocity.

The numerical solution of the electron Boltzmann equation uses cross sections to determine the pumping rate constants by way of equation 16.

$$R_{xy} = \int_0^{\infty} \frac{f(\epsilon) Q v(\epsilon)}{\int_0^{\infty} f(\epsilon) d\epsilon} \quad (16)$$

In equation 16, R_{xy} represents the pumping rate constant (cm^3/sec) from level x to level y, Q is the cross section (cm^2) for that transition, $v(\epsilon)$ is the velocity of the electron, and $f(\epsilon)$ is the electron energy distribution function.

Before the electron energy distribution can be used to calculate pumping rate constants, the cross sections for the excitation and ionization of each gas species must be determined. The next chapter is devoted to the calculation of appropriate cross sections for the Hg/Cl₂/Ar mixture.

III. Cross Sections

Overview

In this chapter, the cross sections necessary for calculating pumping rates from the electron Boltzmann equation are developed. The two major processes discussed are those of electron collisional excitation and electron collisional ionization.

Of the three gases in the HgCl laser, Hg/Cl₂/Ar, Hg cross sections are analyzed in detail. Cross sections for the Argon reactions have been previously determined. These values are listed in the Argon section of this chapter. The section for the cross section by dissociative attachment of Cl₂ treats the process as a narrow function occurring around zero energy.

Some of the cross sections determined in this chapter are a result of direct experimental measurement, while others are the result of solutions to theoretical and experimental equations. The next section is the development of the Hg cross sections.

Mercury (Hg)

Introduction. A metastable level is by definition (Ref 8) a state of an atom which cannot transition to a lower state with the emission of radiation, and correspondingly, cannot be reached from a lower state by absorption. Various transition rules prohibit these "forbidden

transitions". If this transition does occur by some other method than photon absorption, i.e., collisions of the first kind, the result is an extremely long lifetime for the excited atom. In some cases, lifetimes of milliseconds are not uncommon. Transitions caused by collisions of the first kind or collisions of the second kind are prohibited only by the Pauli principle. Because of this type of interaction, evaluation of the entire energy level structure is important.

An atom may be collisionally excited into a metastable state, and, before being radiatively deexcited, collisionally reexcite into a higher energy level. The lifetime of this higher level may be short, causing the atom to deexcite back into the metastable state. This process can occur numerous times before the atom changes its condition by some other process. The atom behaves as if it is storing energy. If a secondary electron collides with this atom, while it is in the higher state, the atom may be collisionally stripped (ionized) of its electron. In essence, an atom capable of being in a stored energy condition, very often behaves as being in a metastable state of the higher energy.

A typical energy level diagram with spectral lines for the element Hg is borrowed from Herzberg (Ref 8) and illustrated in Figure 4.

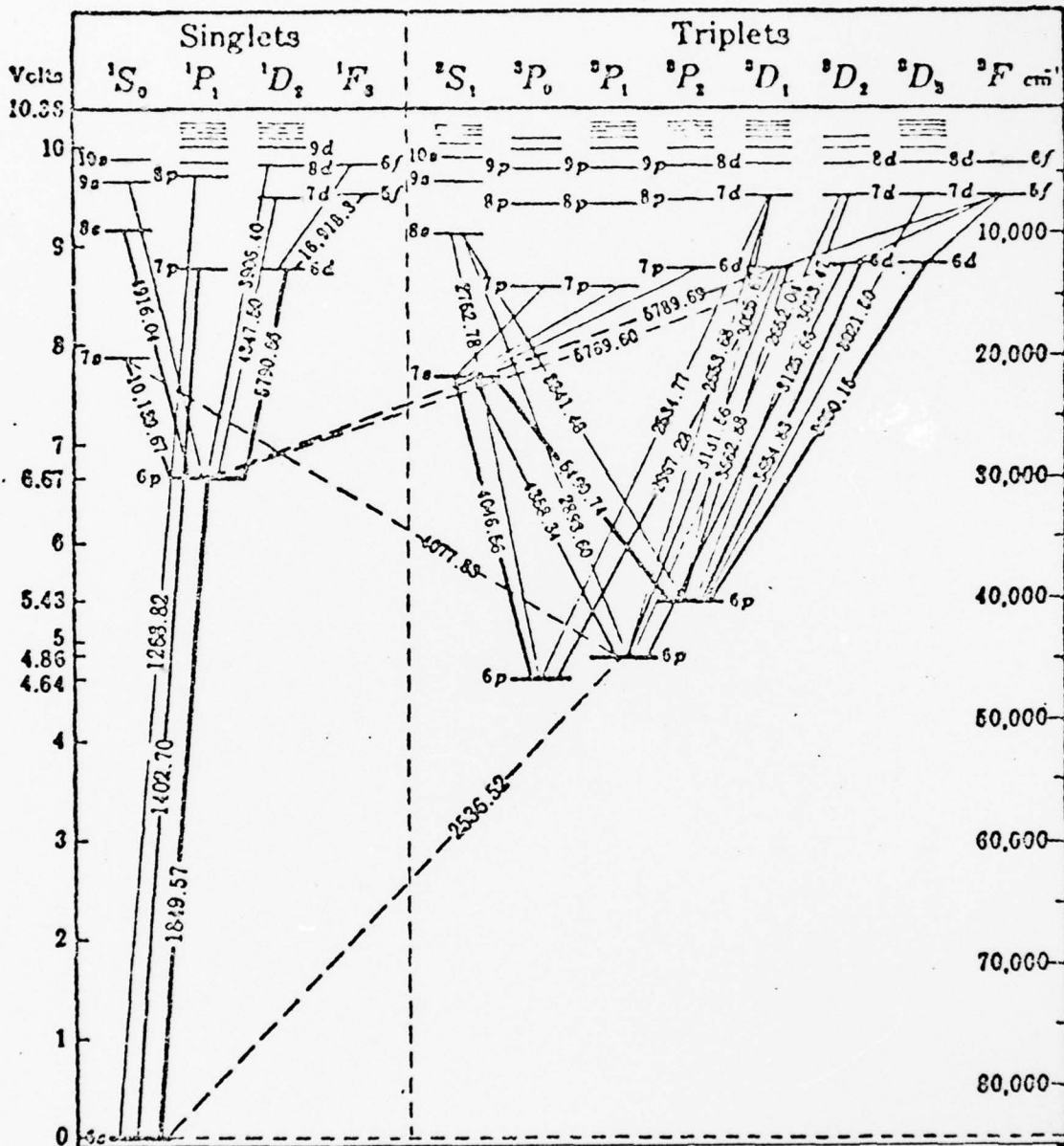


Fig. 4. Relevant Energy Levels for the Hg System. Heavy lines indicate high transition probabilities. No line is a forbidden transition (Ref 8).

Table I lists the probabilities of 17 various transitions for the element Hg.

Table I
Transition Probabilities

Transition	A(j,k)(sec)	Transition	A(j,k)(sec)
$7^3P_2 - 7^3S_1$	0.44	$7^3S_1 - 6^3P_2$	1.1
$7^3P_1 - 7^3S_1$	0.18	$7^3S_1 - 6^3P_1$	1.2
$7^3P_0 - 7^3S_1$	0.23	$7^3S_1 - 6^3P_0$	0.52
$7^3P_1 - 7^1S_0$	0.035	$7^3S_1 - 6^1P_1$	0.002
$7^1P_1 - 7^1S_0$	0.18	$7^1S_0 - 6^1P_1$	0.29
$7^1P_1 - 7^3S_1$	0.15	$7^1S_0 - 6^3P_1$	0.13
$7^3P_1 - 6^1S_0$	0.13	$6^3D_2 - 6^3P_2$	0.54
$7^1P_1 - 6^1S_0$	0.37	$6^3D_2 - 6^3P_1$	3.30
		$6^3D_2 - 6^1P_1$	0.16

Transition Probabilities (in units of 10^8Sec^{-1}).
(Ref 9) Limits of error omitted.

For ease of understanding, the radiative lifetimes are computed by,

$$\tau(j,k) = A^{-1}(j,k) \quad (17)$$

and displayed in Figure 5. The units of A are sec^{-1} .

The lifetimes of the $6^3P_{2,1,0}$ level are measured by Panevkin (Ref 10) to be 4×10^{-5} , 1×10^{-5} , and 6×10^{-5} sec respectively. Most of the transitions shown in Figure 5 are fast, occurring between 1×10^{-8} and 1×10^{-9} seconds.

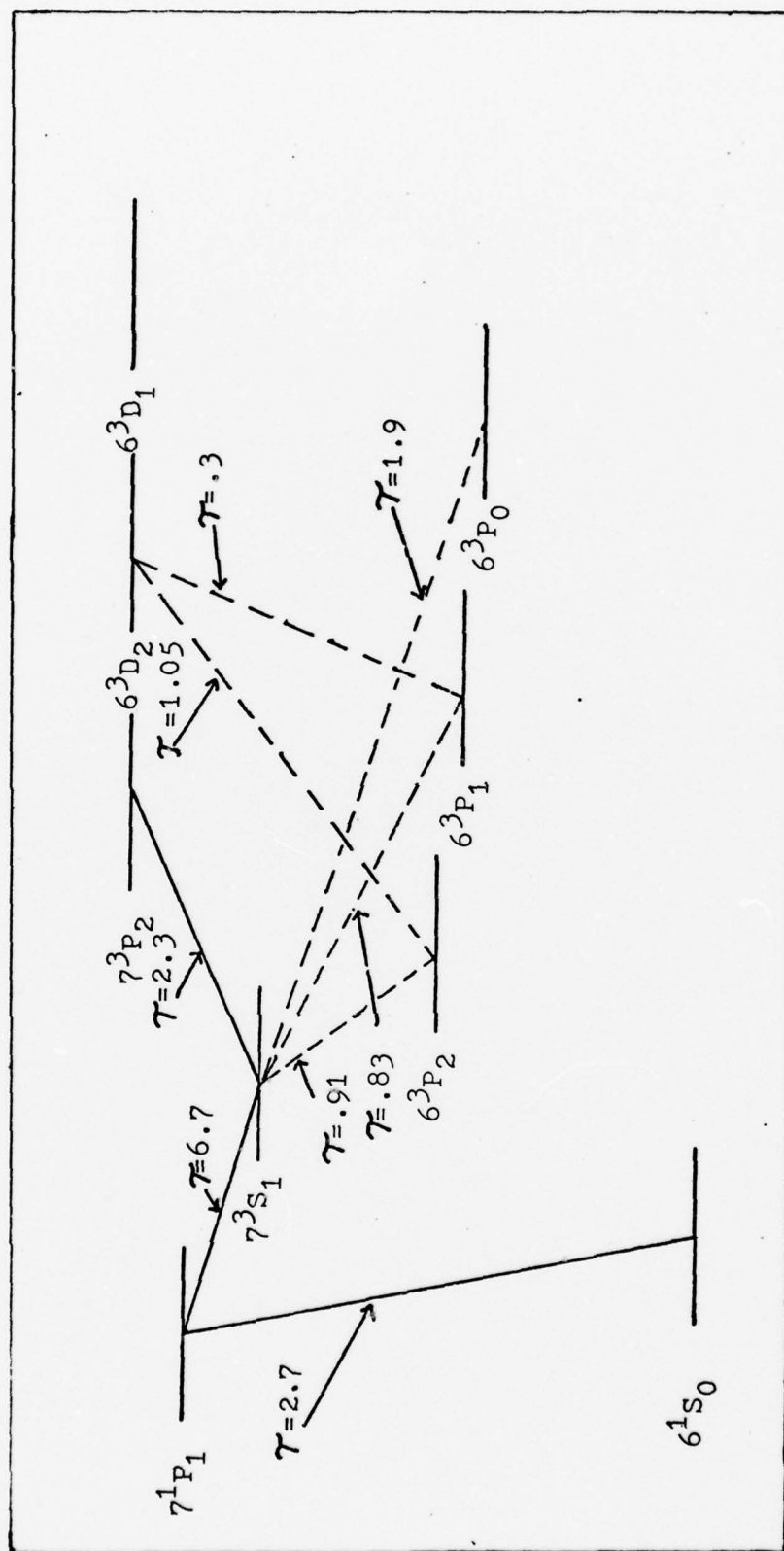


Fig. 5. Broken lines indicate regions of possible stored energy (in units of 10^{-8} sec).

Investigation of the energy level diagram with the associated lifetimes indicates the possibility of trapped radiation between the states $7^3S_1 - 6^3P_{2,1,0}$, $6^1P_1 - 6^1S_0$, and $6^3D - 6^3P_{2,1}$. The high transition probability and the long lifetimes of the lower states are good indicators.

Rockwood (Ref 5) and Tang (Ref 11) recognize the need to consider higher excited levels of Hg other than the $3P_{2,1,0}$ level. These higher excited levels may act as metastable states, capable of being ionized by secondary electrons.

In order to arrive at more accurate results, the temporal evolution of these excited levels needs to be tracked. The next section develops the cross sections necessary for following these levels. The notation and corresponding energy level is tabulated in the following list.

<u>Notation</u>	<u>State</u>	<u>Level (eV)</u>
Hg [*]	6^3P_2	5.46
Hg ^{**}	6^1P_1	6.70
Hg ^{***}	7^3S_1	7.73
Hg ^{****}	6^3D_2	8.85

The reason for tracking the 6^3P_2 level instead of all three 6^3P levels is mainly for simplicity and ease of calculations. A quantitative argument for tracking only the 6^3P_2 level is made in the results section of this chapter.

Theory

Electron Impact Excitation

A pumping rate constant is only as good as the cross section which determines that rate constant. Cross section curves can be calculated with quantum mechanical methods; however, the calculations are extremely complicated and require approximations that make the degree of accuracy almost impossible. An appreciation of this difficulty is evident in the work of Yavorsky (Ref 12). He calculates, quantum mechanically, the cross section for the $6^3P_1 - 6^3P_2$ Hg transition by a free electron.

Fortunately, Bauer and Bartkly (Ref 13) show that classical theory is often adequate for determining collisional cross sections. This technique works best when the free electron is below 27 eV ($e^2/hv \gg 1$).

A classical differential cross section is defined by,

$$\sigma = d Q_n / d\epsilon \quad (18)$$

In equation 18, ϵ is the energy (eV) transferred from the incident electron to the orbital electron, Q_n (cm^2/eV) represents the total cross section for transition n . An integration over the limits of energy needed to reach a level (U_{n+1}) yields a total cross section as in equation 19. The upper limit of integration is determined by the energy necessary to reach the next highest energy level.

$$Q_n = \int_{U_n}^{U_{n+1}} \sigma_n(\epsilon) d\epsilon \quad (19)$$

With the approach of equation 19, Bauer and Bartkly (Ref 13) examine several theoretical and empirical solutions for the differential cross section $\sigma(\epsilon)$. In particular, they cite the work of Thompson (Ref 14), Drawin (Ref 15), a series of papers by Gryzinski, one of which is Ref 16, and Ochkur and Petrun'kin (Ref 17). Bauer and Bartkly state that their results agree with experimental data, where available, within a factor of 3.

Equations 20 and 21 are two solutions they find agreeable with experimental results. Equation 20 is known as the Thompson formulation and equation 21 as the Gryzinski formulation.

$$Q_1(E_2) = \left(\frac{N_e \pi e^4}{U_n} \right) \xi_1(E_2, I, U_n, U_{n+1}), \quad (20a)$$

where

$$\xi_1 = \begin{cases} \frac{U_n^2 (E_2 - U_n)}{(E_2 + I)(E_2 + I - U_n)I}, & U_n \leq E_2 \leq U_{n+1} \\ \frac{U_n^2 (U_{n+1} - U_n)}{(E_2 + I)(E_2 + I - U_n)(E_2 + I - U_{n+1})}, & E_2 \geq U_{n+1} \end{cases} \quad (20b)$$

$$Q_2(E_2) = (N_e \pi e^4) \xi_2(E_2, I, U) \delta'U, \quad (21a)$$

where

$$\xi_2 = \left\{ \frac{E_2 + I - U_n}{I} + \left[\frac{4}{3} - \left(\frac{E_2 + I - U_n}{E_2 + I} \right) \ln \left(2.72 + \sqrt{\frac{U_n}{I}} \right) \right] \right\} \left[\frac{1}{(E_2 + I - U_n)^3} - \frac{I}{(E_2 + I)} \right] \quad (21b)$$

$$\left[\frac{E_2 + I}{E_2 + 2I} \right]^{3/2} \left[\frac{U_n}{E_2 + I} \right] \left(\frac{I}{2I + E_2 - U_n} \right)$$

and

$$\delta'U = \begin{cases} E_2 - U_n & , & U_n < E_2 < U_{n+1} \\ U_{n+1} - U_n & , & E_2 \geq U_{n+1} \end{cases}$$

In equations 20 and 21, E_2 is the energy (eV) of the incident electron, I (eV) is the ionization potential of the state from which the atom is excited, U_n (eV) and U_{n+1} (eV) are the bottom and top energies of the excited level, and N_e is the equivalent number of electrons.

The equivalent number of electrons (N_e) is an adjustable parameter that can take on several values, depending on the process in question. For electron exchange

processes, Bauer and Bartkly recommend N_e equal to $\frac{1}{2}$.

Bauer and Bartkly also identify some of the problem areas of equations 20 and 21. The function in equation 20 fits better in the lower energy region, but drops off more rapidly than equation 21 in the high energy region. Either equation compares reasonably well with experiment, and the authors feel the results will always be within a factor of 4 of experimental data.

Electron Impact Ionization

The electron ionization cross section formula developed by Gryzinski is used throughout the Bauer and Bartkly article. They feel the Gryzinski equation agrees best with experimental data. The formula is shown in equation 22.

$$Q_I = N_e \frac{\pi e^4}{I^2} g_I \left(\frac{E_2}{I} \right), \quad (22a)$$

where

$$g_I(X) = \frac{1}{X} \left(\frac{X-1}{X+1} \right)^{3/2} \left[1 + \frac{2}{3} \left(1 - \frac{1}{2X} \right) \ln(2.72 + \sqrt{X-1}) \right], \quad X = \frac{E_2}{I} \quad (22b)$$

In equation 22, E_2 is the energy of the incident electron, and I (eV) is the energy necessary for ionization.

Vrien (Ref 18) develops a much simpler ionization cross section equation that compares very well with experimental data. The results are shown in equation 23.

$$Q_I = \frac{740\pi a_0^2}{E+3.25I} \left(\frac{1}{I} - \frac{1}{E} \right) + \frac{2I}{E} \left(\frac{1}{I^2} - \frac{1}{E^2} \right) \quad (23)$$

In equation 23, E is the incident electron energy, I(eV) is the energy necessary for ionization and πa_0^2 equals $0.88 \times 10^{-16} \text{cm}^2$. This formula works best when the energy for ionization is less than 3.5 ev.

Equations 20 through 23 are all the equations necessary for determining pumping rates by the numerical solution of the electron Boltzmann equation of Chapter 1. The next section calculates the cross sections for Mercury and compares them with experimental data, when available. The cross sections eventually used in the numerical calculations of the discharge in Chapter 4 are identified in the summary section of this chapter.

Results

Rockwood (Ref 5) and Cayless (Ref 19) show the cross sections for the $6^1S_0 - 6^3P_{2,1,0}$ transition. The results are illustrated in Figures 6 and 7, respectively.

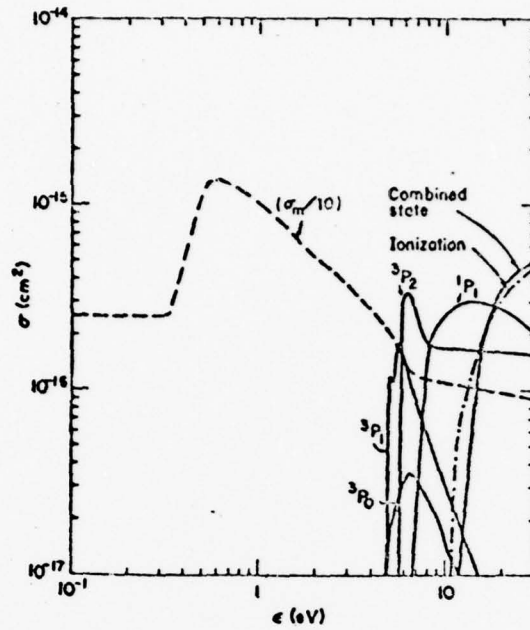


Fig. 6. Elastic and inelastic-scattering cross sections for electrons in Hg as a function of energy (Ref 5).

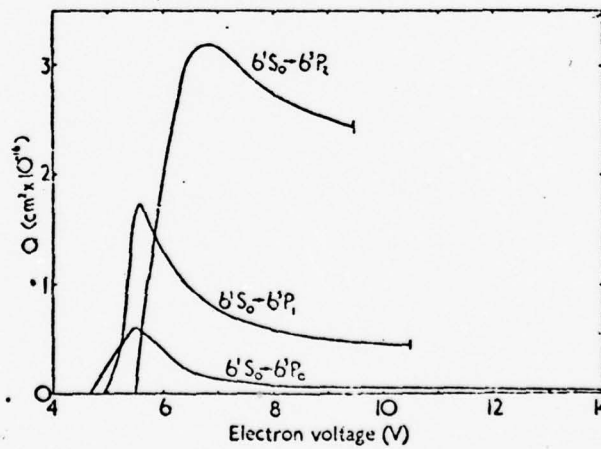


Fig. 7. Excitation cross-sections for the 6^3P levels of Hg (Ref 19).

The pumping rate constant for a specific collisional process, when weighed by the velocity, is proportional to the area under the curve. It is evident that the $6^1S_0-6^3P_2$ cross section is several times greater than the cross section for the $6^1S_0-6^3P_{1,0}$ transition. This is the reason that only the $6^1S_0-6^3P_2$ transition is tracked. To be completely correct the other transitions should be included, along with the reactions among the $6^3P_{2,1,0}$ level. (See Appendix A).

The Gryzinski equation of the previous section is used to calculate the $6^1S_0-6^3P_2$ transition. The results are shown in Figure 8. Note the fall off at high energy which may cause an underestimation in the total pumping rate. An equivalent number of electrons of 20 is needed to bring the curve up to the same order of magnitude as the curves of Rockwood (Ref 6) and Cayless (Ref 19). This value is suspect, but no other method is available for a comparison. At worst, the results are correct to an order-of-magnitude.

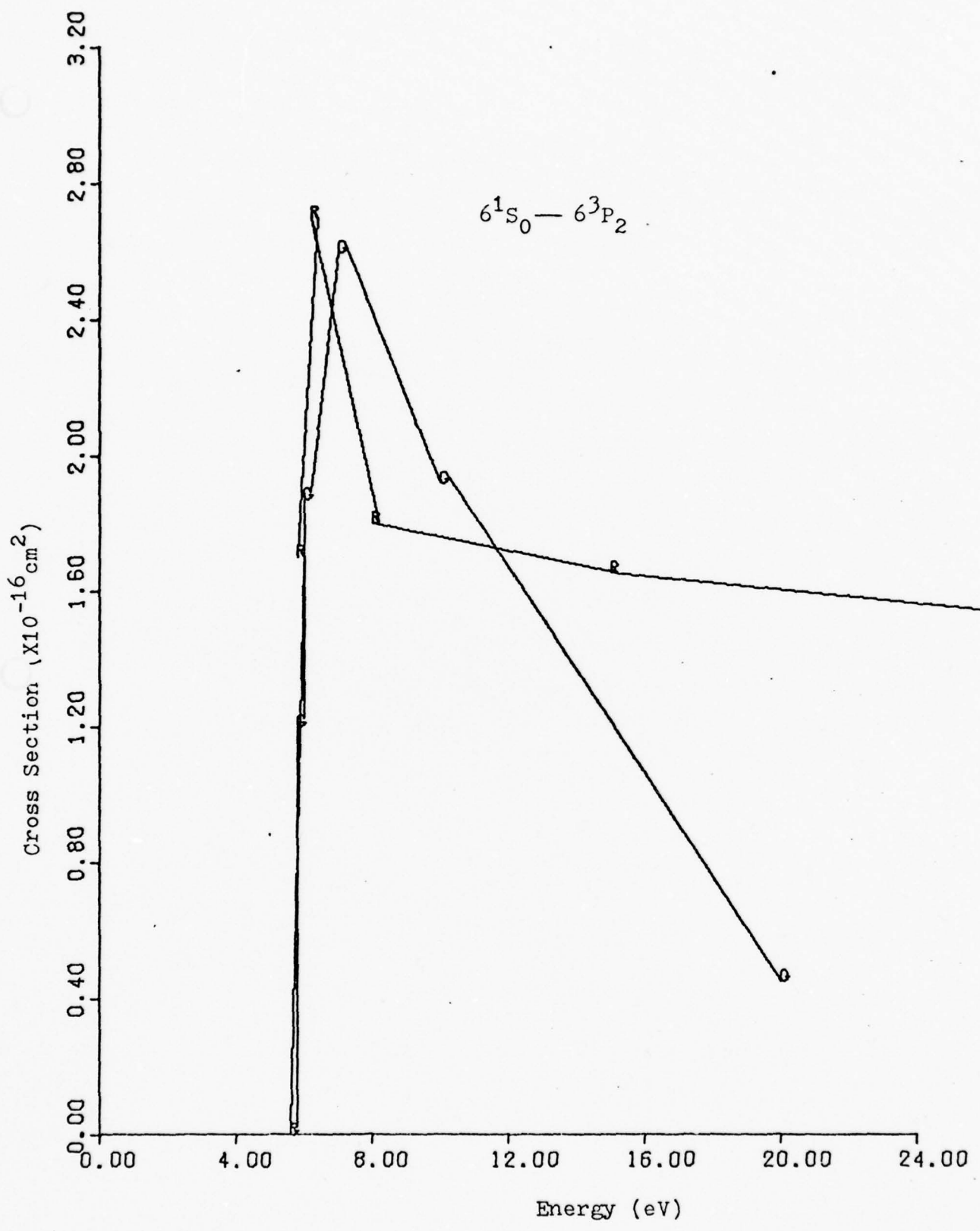


Fig. 8. Calculated cross section from Gryzinski (G) and Rockwood (R).

The $6^1S_0 - 6^1P_1$ transition of Rockwood (Ref 5) and Cayless (Ref 19) are shown in Figures 6 and 9, respectively.

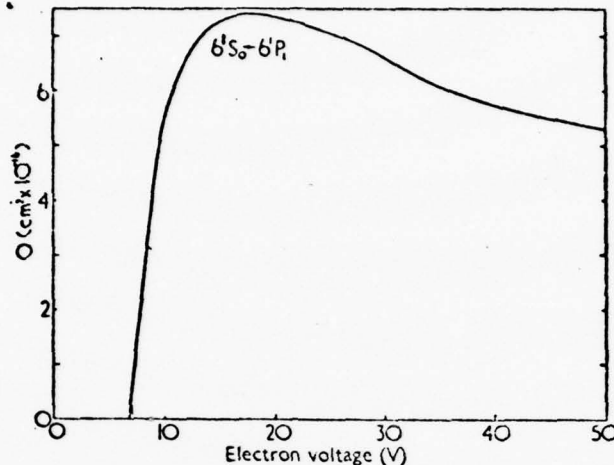


Fig. 9. Excitation cross-section for 6^1P_1 for Hg.

A comparison with equations 19 and 20 of the previous section require an equivalent number of electrons (N_e) of 20 to bring the calculated curve within an-order-of-magnitude of Figure 9.

The $6^1S_0 - 7^3S_1$ transition cross section is determined by Yavorski (Ref 12) and used by Cayless (Ref 15). This cross section is shown in Figure 10.

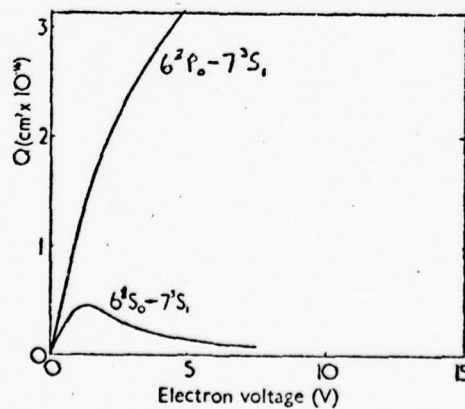


Fig. 10. Cross-sections for excitation of 7^3S_1 from the ground state and 6^3P_0 of Hg, after Yavorski. (Origin transposed)(Ref 15).

A collisional cross section for the $6^3P_2 - 7^3S_1$ transition is shown in Figure 11. The curve is a result of the work of Korotkov and Kazakov - furnished by Garscadden (Ref 17).

Cross sections for the remaining excitation transitions are not found in the literature. The Gryzinski solution is used and the results shown in Figures 12 through 17.

Any pumping rate determined from these collisional excitation cross sections can be incorrect by an order of magnitude. Part of this is due to the behavior of the cross section in the high energy region. If the cross sections for transfers within the triplet or singlet region of the energy level diagram behave as the cross sections calculated by Korotkov and Kazakov (Ref 17), the predicted cross section calculated by Gryzinski is too low in the higher energy region. Until experimental data can determine these excited cross sections, a full understanding of the microscopic processes is highly speculative.

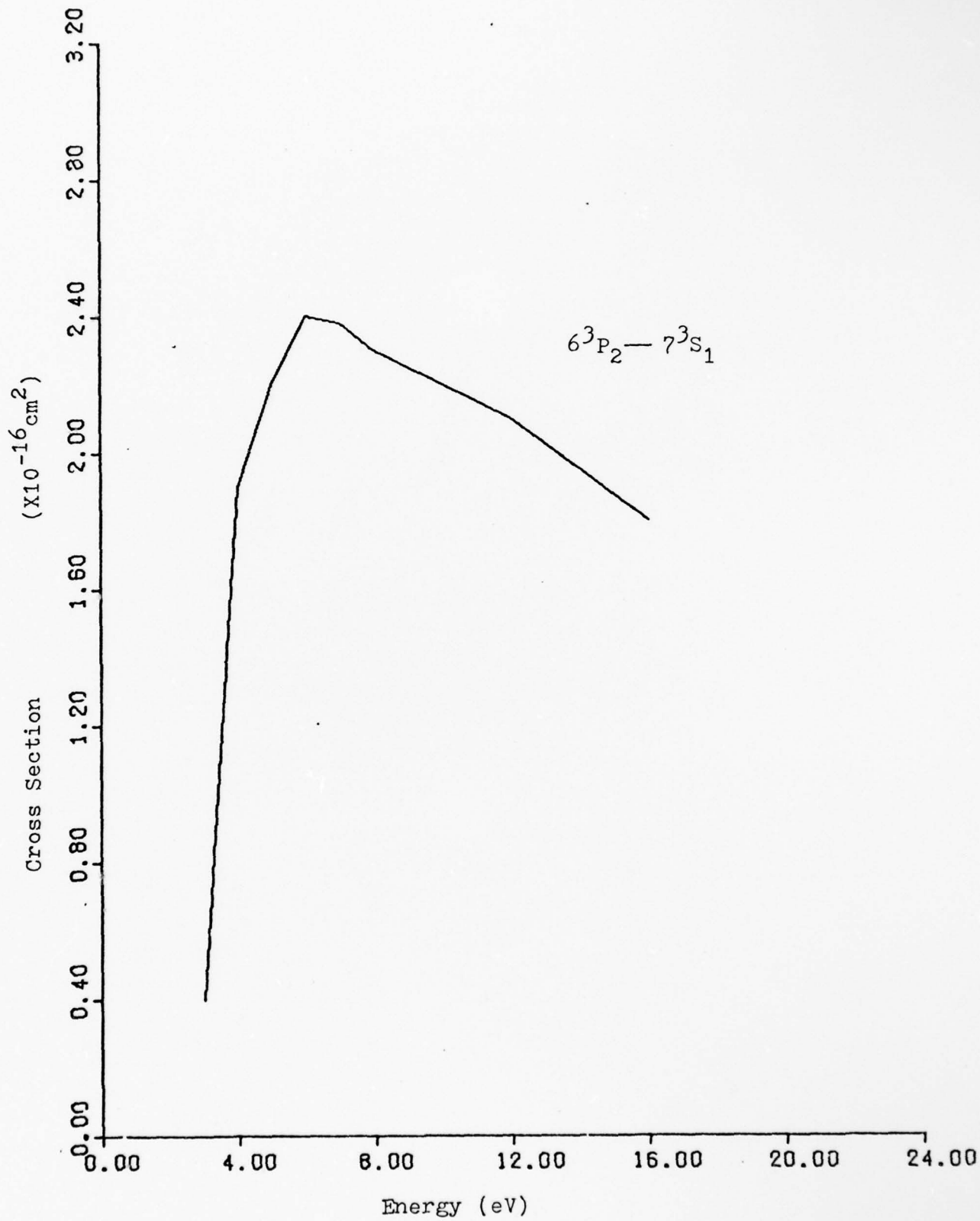


Fig. 11. Excitation of Mercury by electron impact $6^3P_2 - 7^3S_1$ (Ref 17).

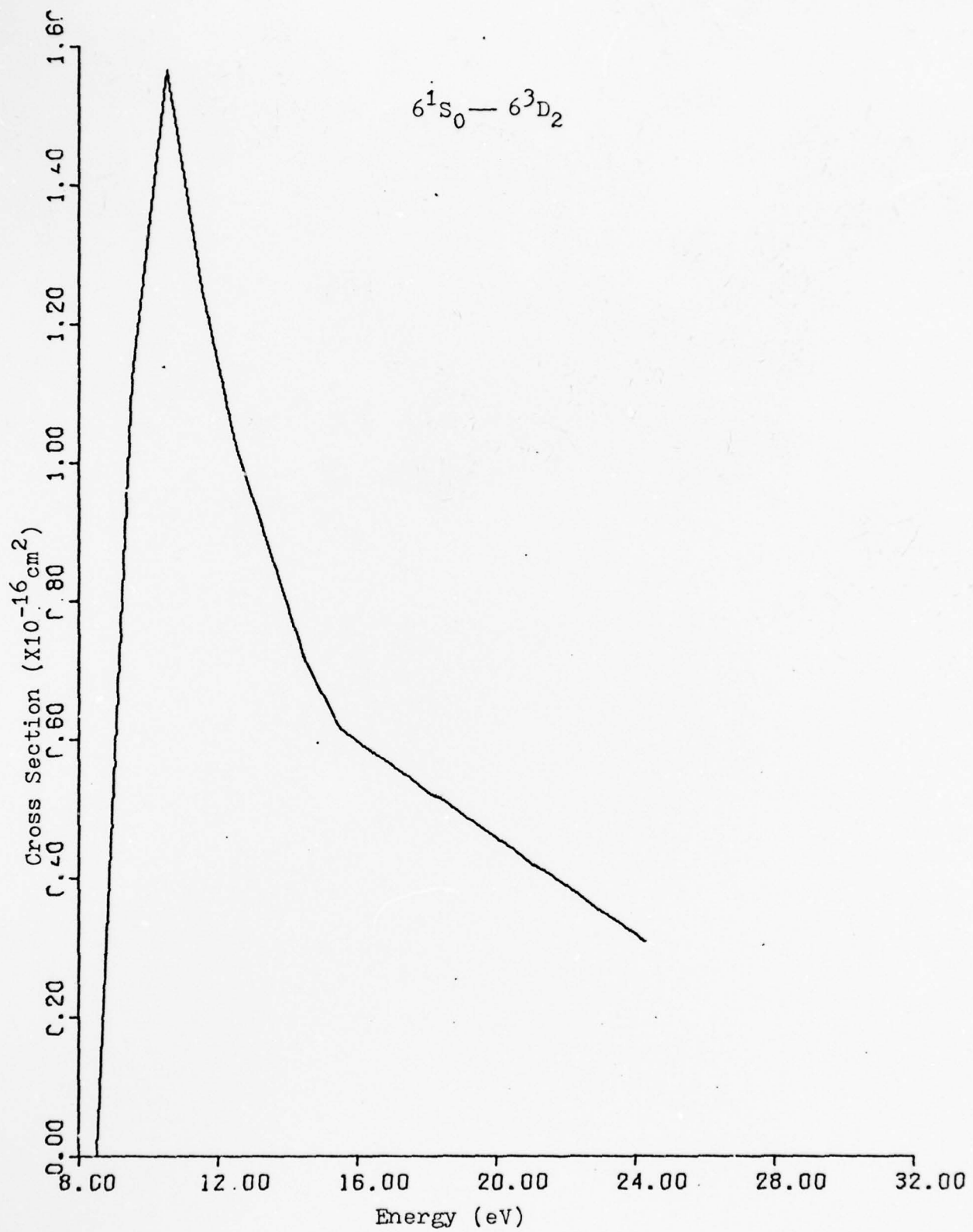


Fig. 12. Excitation of Mercury by electron impact.

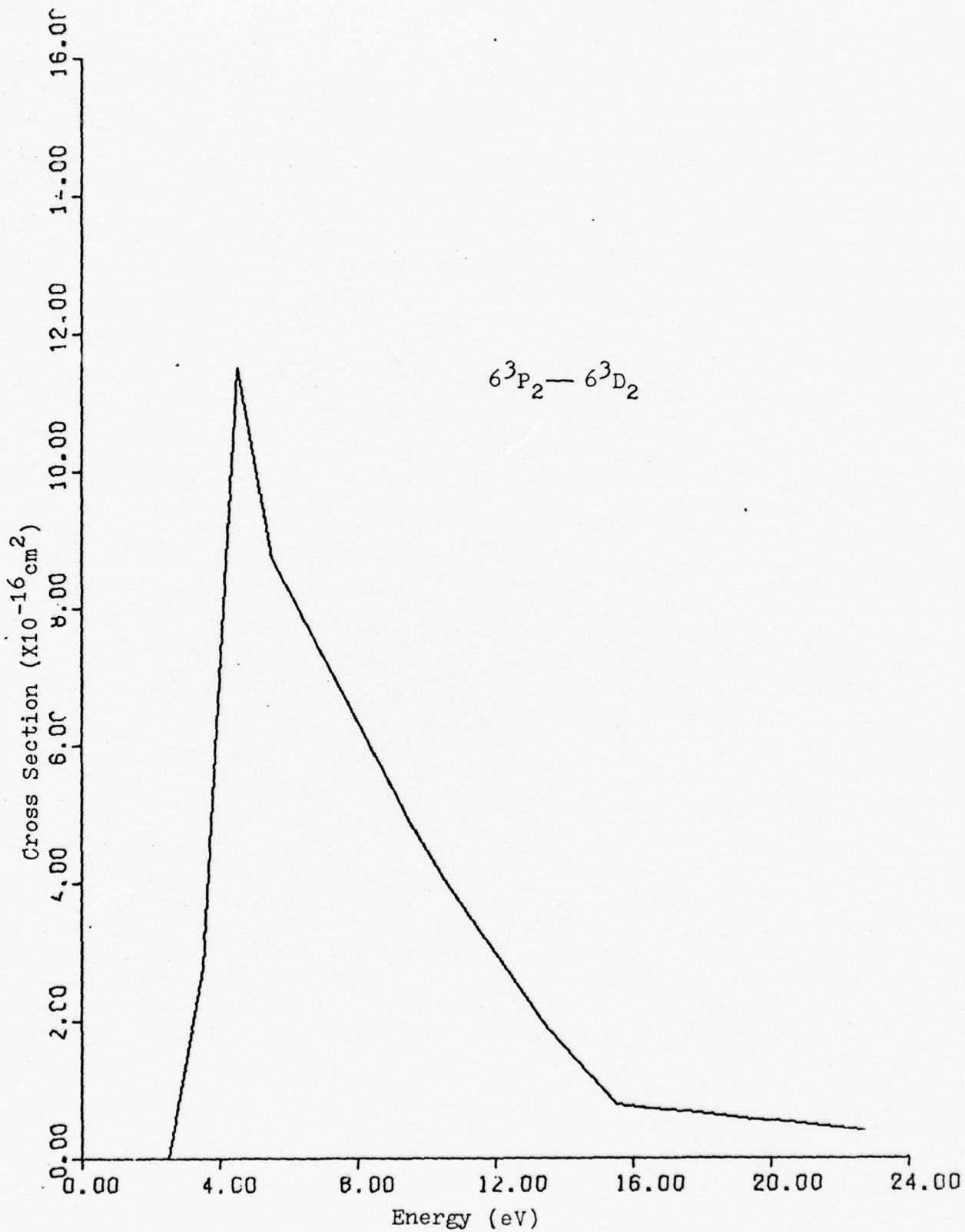


Fig. 13. Excitation of Mercury by electron impact.

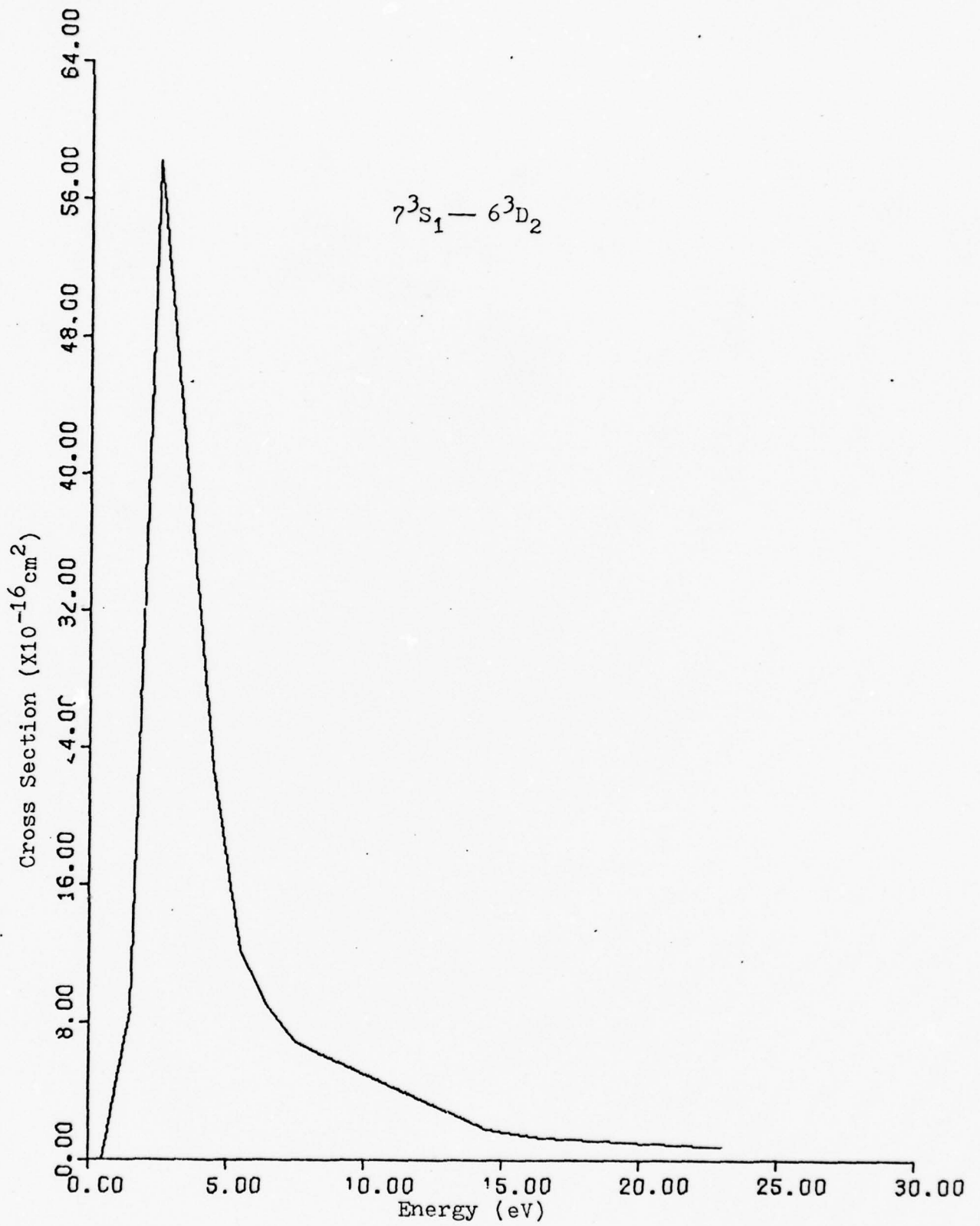


Fig. 14. Excitation of Mercury by electron impact.

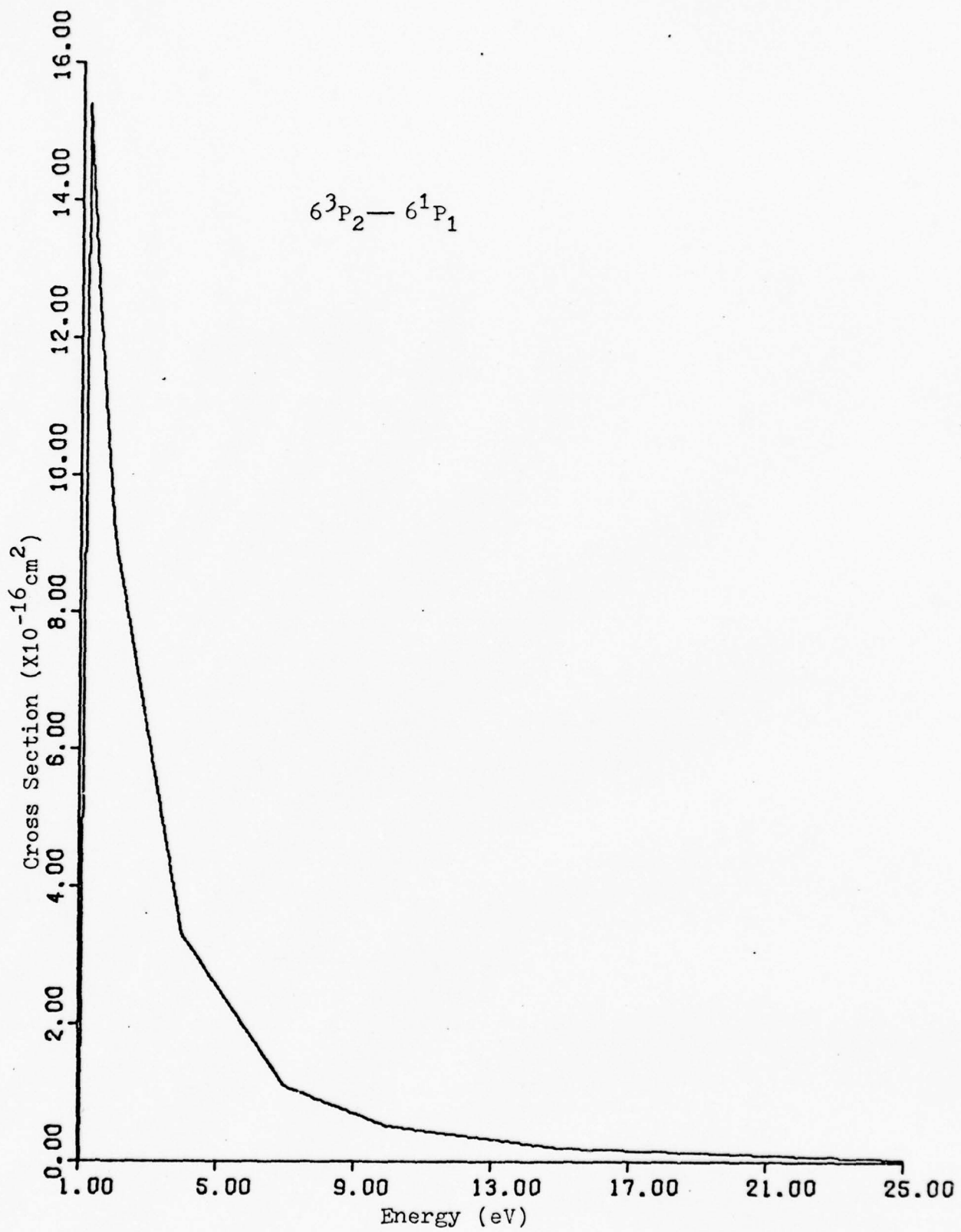


Fig. 15. Excitation of Mercury by electron impact.

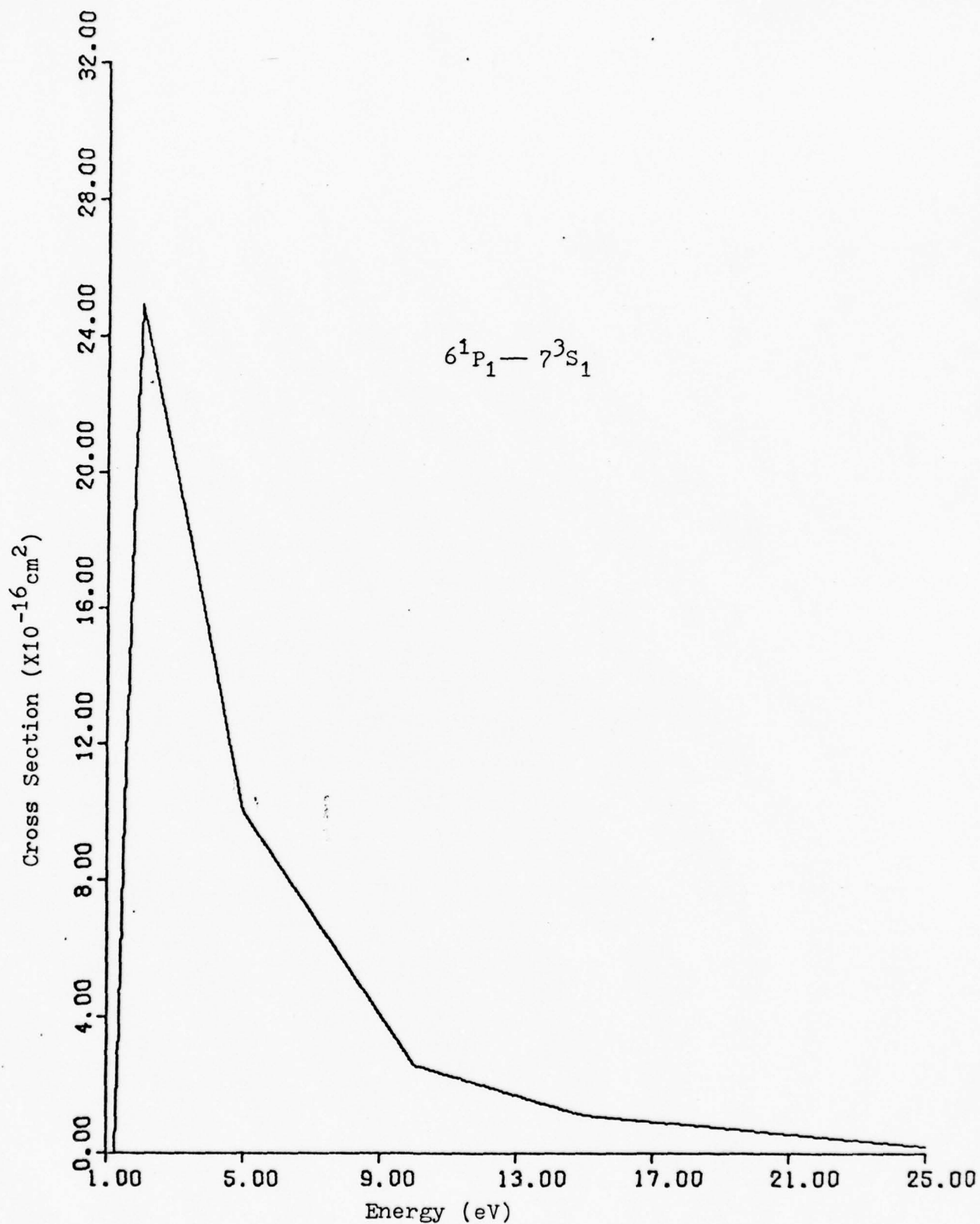


Fig. 16. Excitation of Mercury by electron impact.

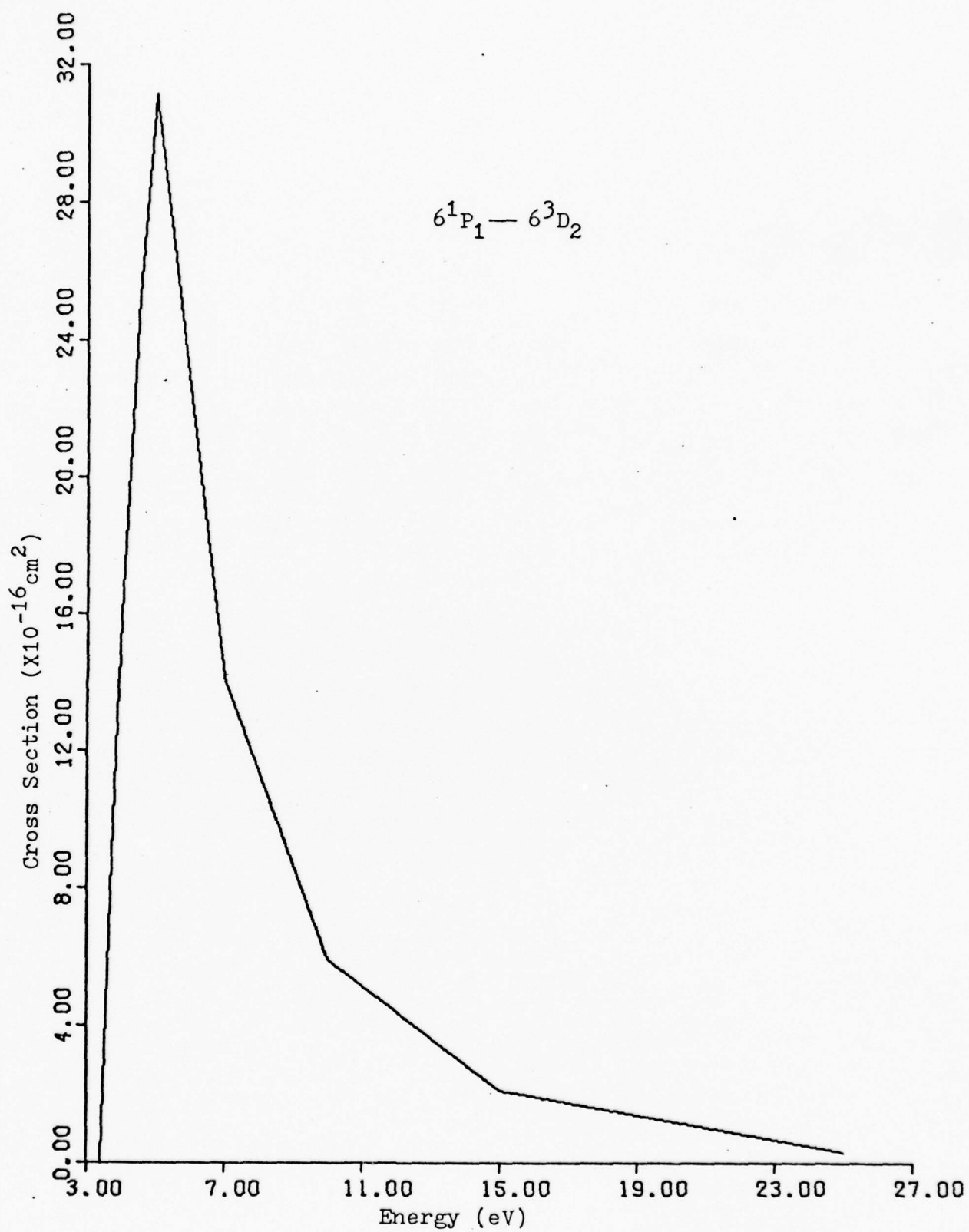


Fig. 17. Excitation of Mercury by electron impact.

Rockwood (Ref 5) uses the ionization cross section shown in Figure 6. This result is very similar to the ionization cross section used by Cayless (Ref 19). Figure 18 shows the ionization cross sections using the Gryzinski equation and the Vrien equation.

Ionization cross sections of higher metastable levels of Hg are not available in the literature. Their values are calculated using the Vrien equation and shown in Figures 19 through 22.

The last section of this chapter is a listing of the cross sections used in the numerical solution of the electron Boltzmann equation, and the reference for the evaluation.

Summary

Cross sections not included in the following list can be added when experimental results show a need for their contributions.

Table II lists the reactions utilized by the numerical HgCl discharge program of Chapter 4. The list also provides the reference for determining the cross section.

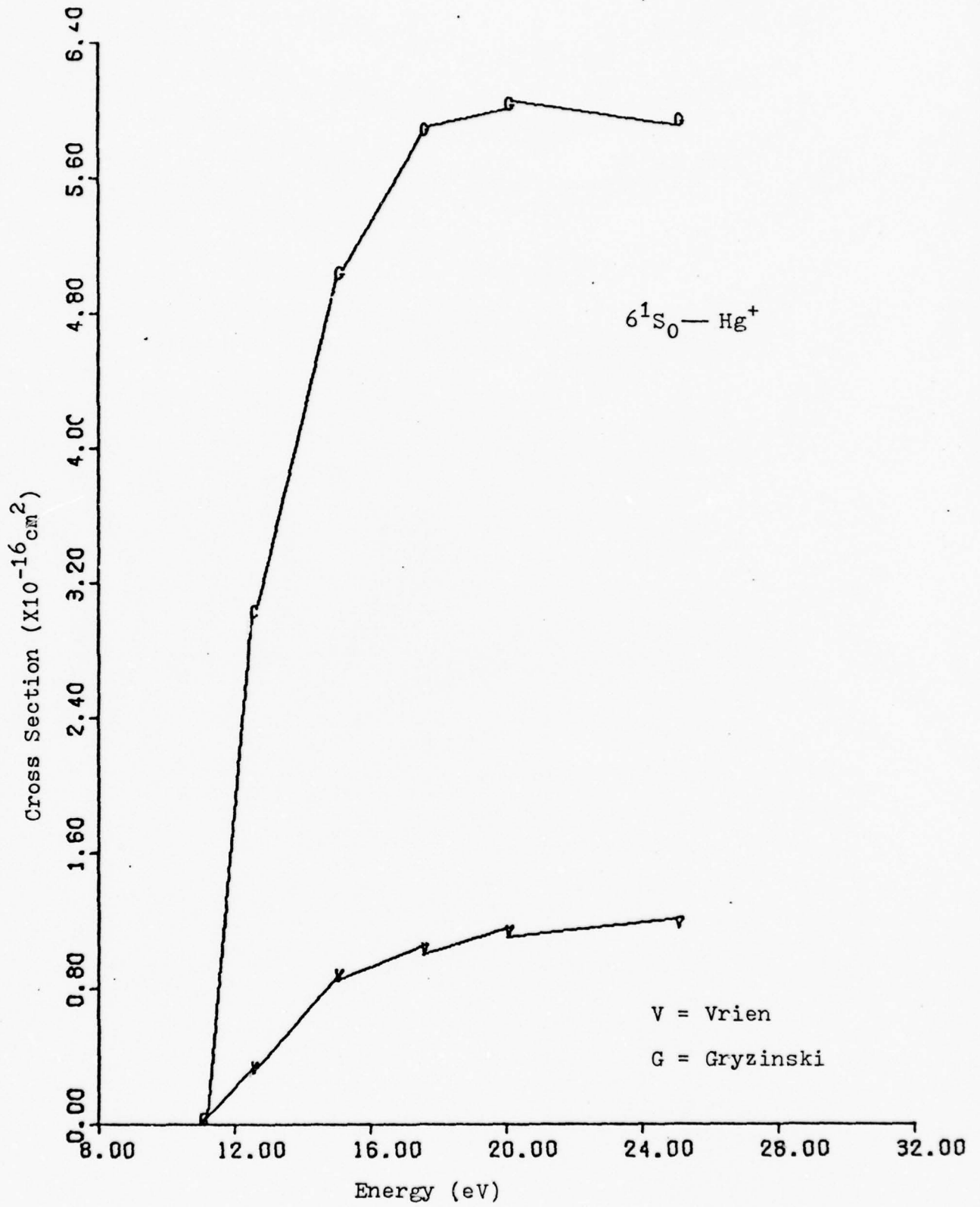


Fig. 18. Ionization of Mercury by electron impact.

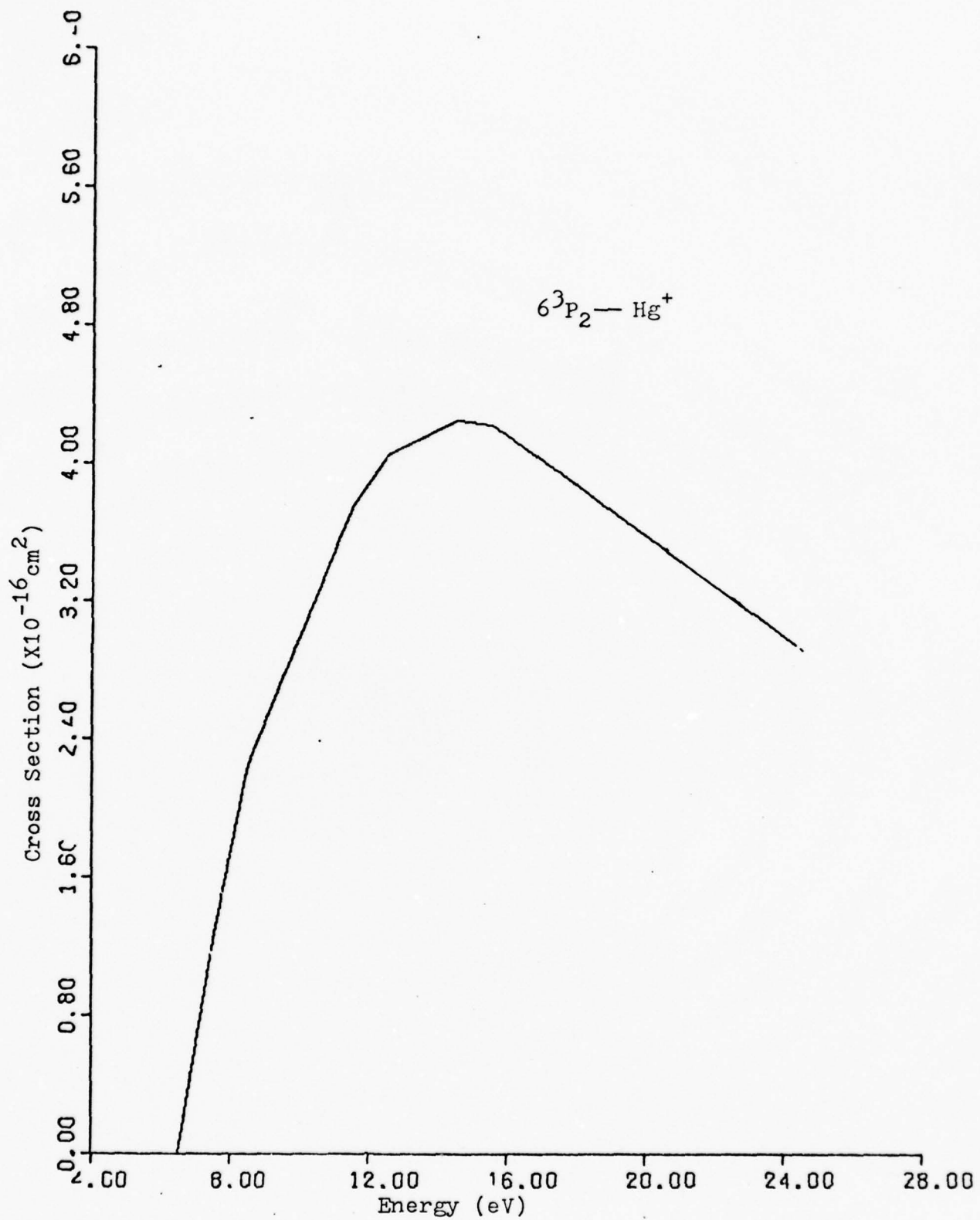


Fig. 19. Ionization of Mercury by electron impact.

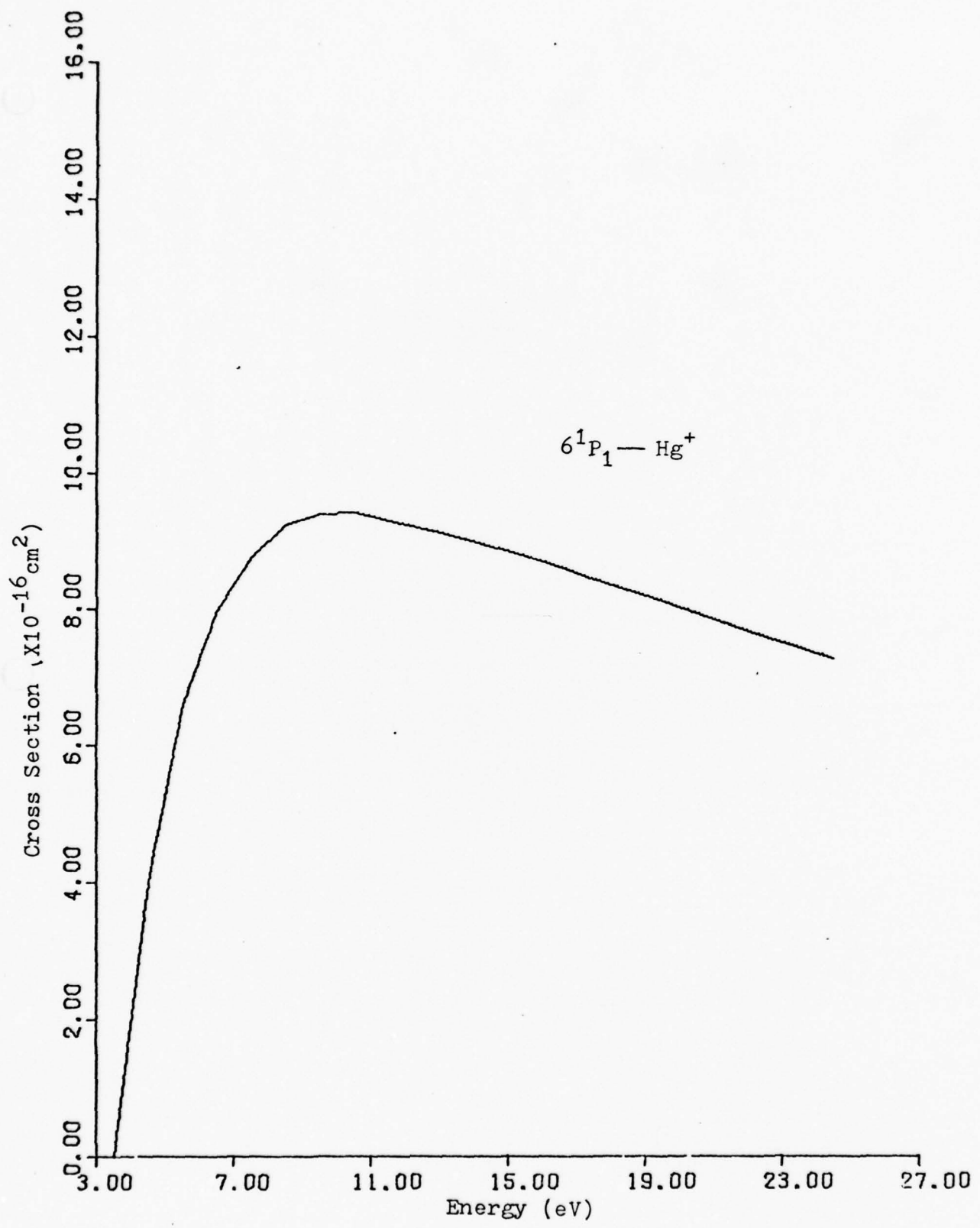


Fig. 20. Ionization of Mercury by electron impact.

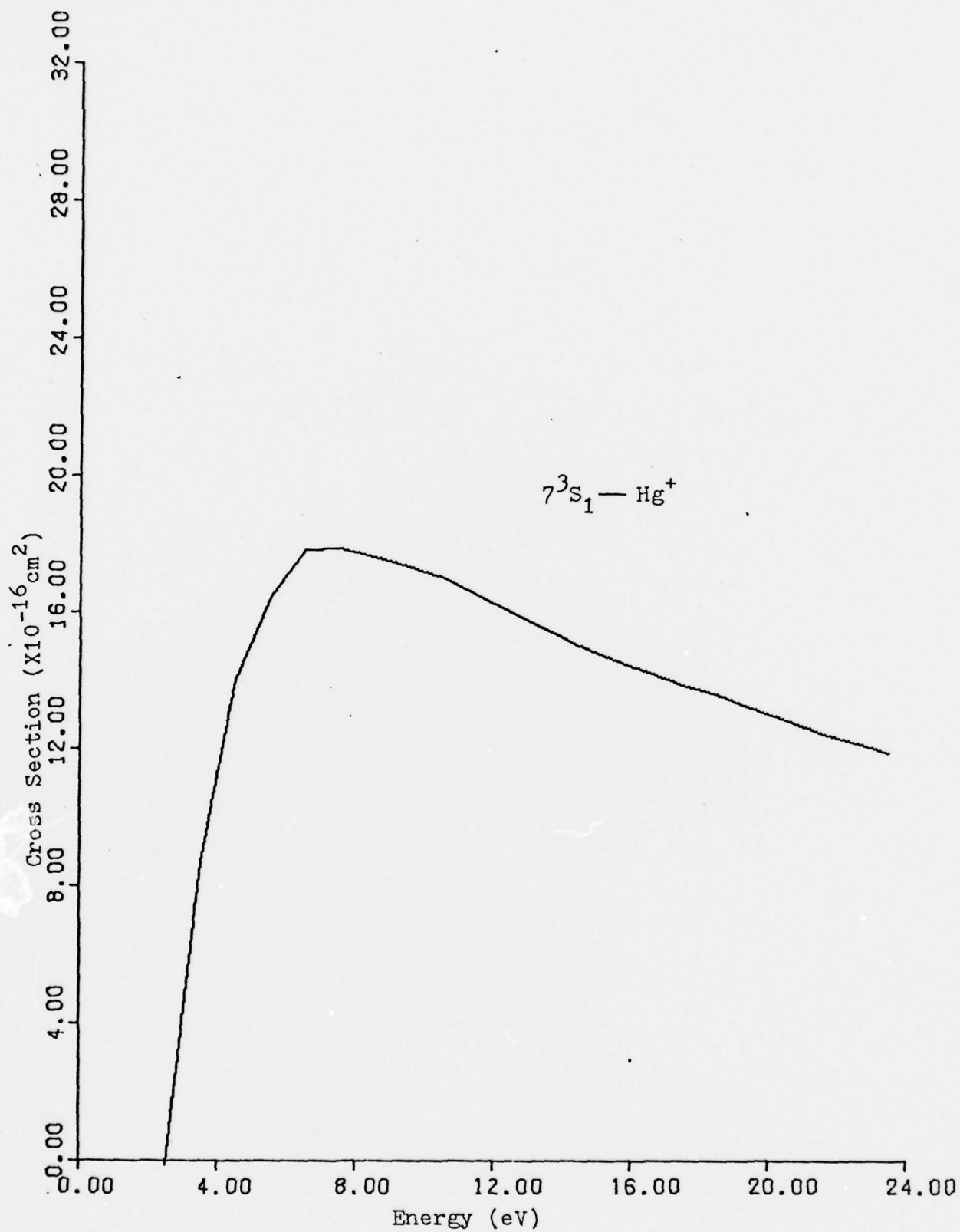


Fig. 21. Ionization of Mercury by electron impact.

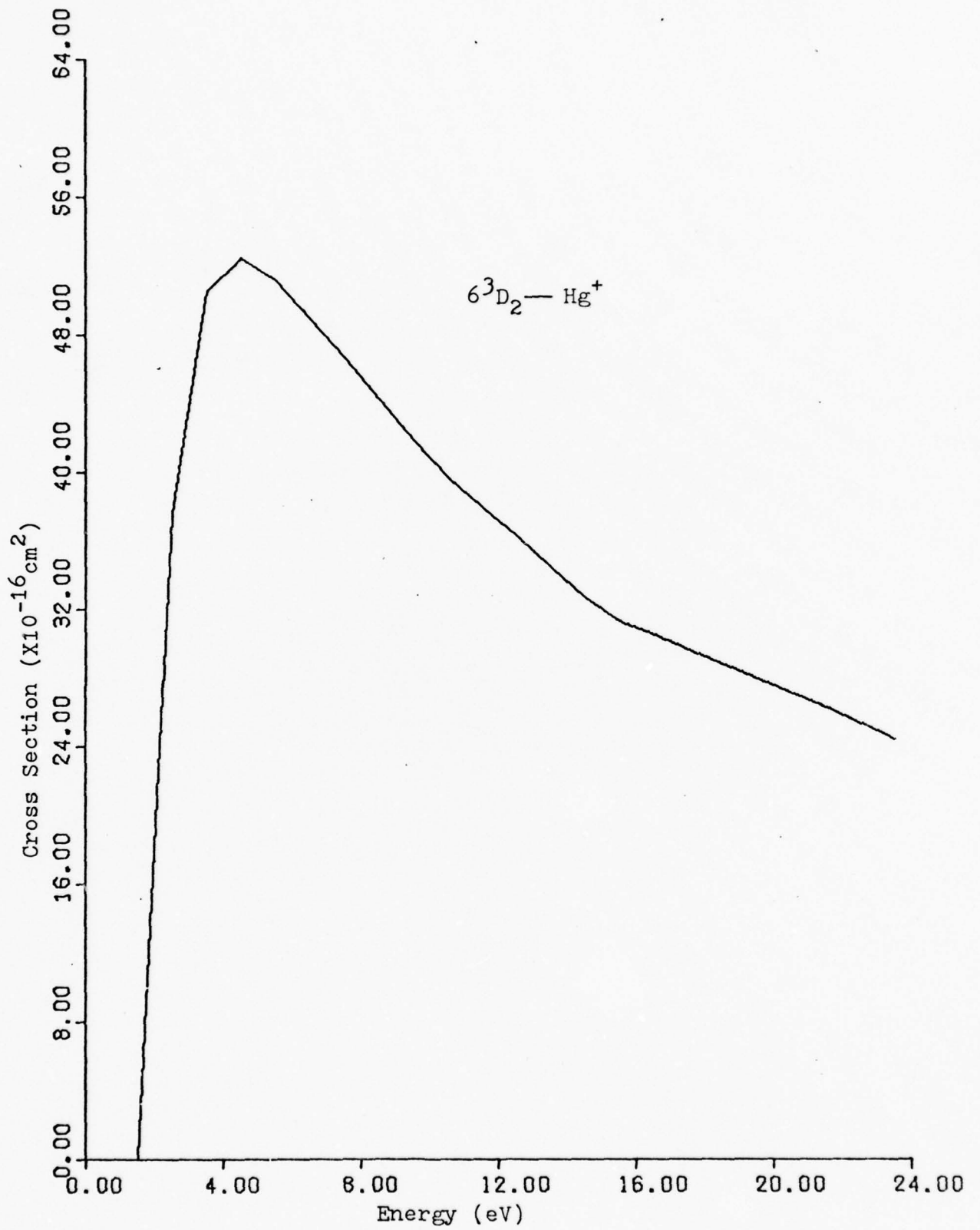


Fig. 22. Ionization of Mercury by electron impact.

Table II
Mercury Cross Sections

<u>Reaction</u>	<u>Reference</u>
$6^1S_0 - 6^3P_2$	5
$6^1S_0 - 6^1P_1$	5
$6^1P_1 - 6^3P_2$	16
$6^1S_0 - 7^3S_1$	19
$6^1P_1 - 7^3S_1$	16
$6^1S_0 - 6^3D_2$	16
$6^3P_2 - 7^3S_1$	20
$6^3P_2 - 6^3D_2$	16
$7^3S_1 - 6^3D_2$	16
$6^3P_2 - 6^1P_1$	16
$6^1S_4 - Hg^+$	5
$6^3P_2 - Hg^+$	18
$6^1P_1 - Hg^+$	18
$6^3S_1 - Hg^+$	18
$6^3D_2 - Hg^+$	18

The following two sections list the collisional cross sections for the element Ar and the dissociative attachment cross section Cl_2 .

Argon (Ar)

The cross sections for excitation and ionization of mercury are well documented. These values are widely used and considered fairly accurate. The listing, and Figures 23 through 28 show these values.

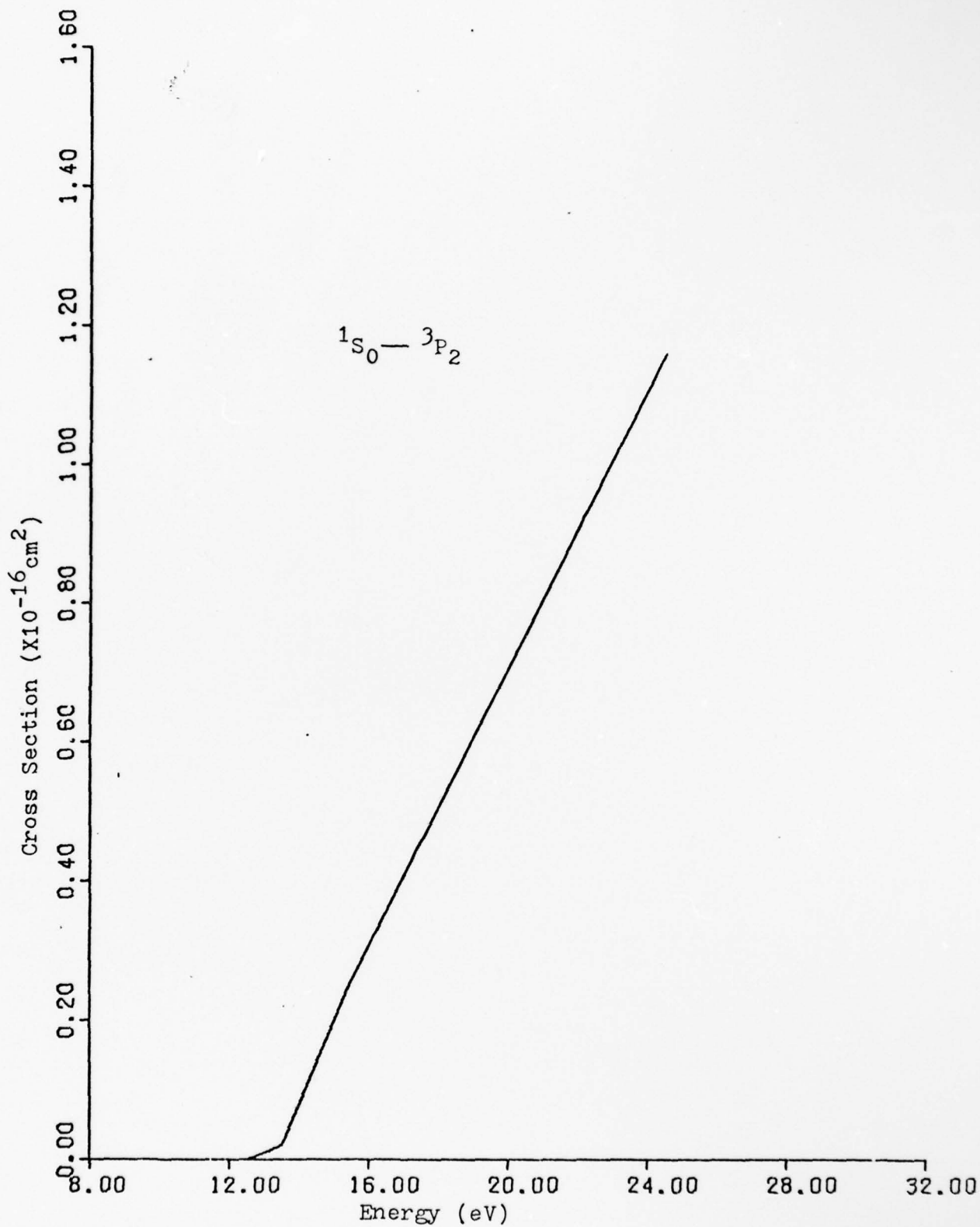


Fig. 23. Excitation of Argon by electron impact.

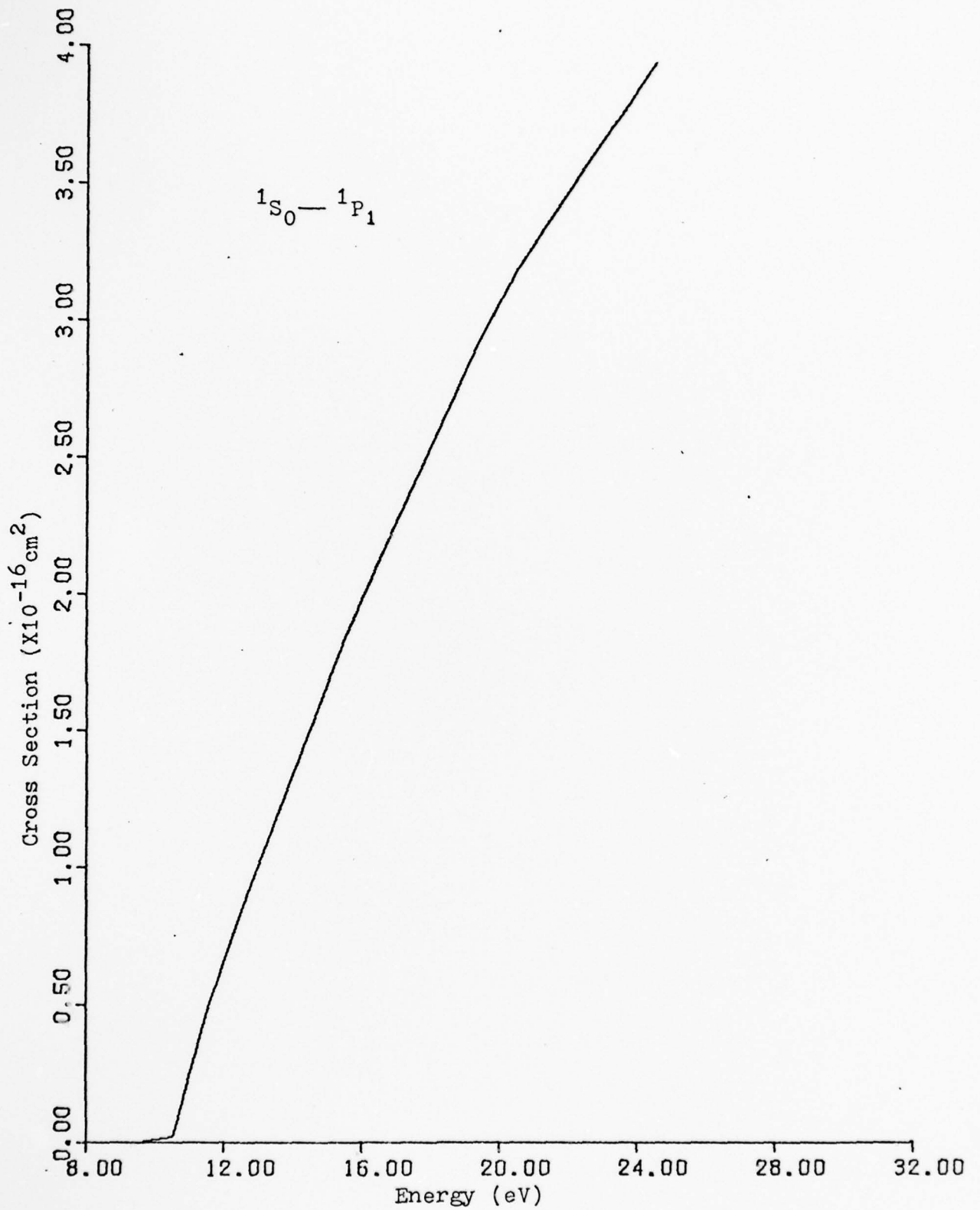


Fig. 24. Excitation of Argon by electron impact.

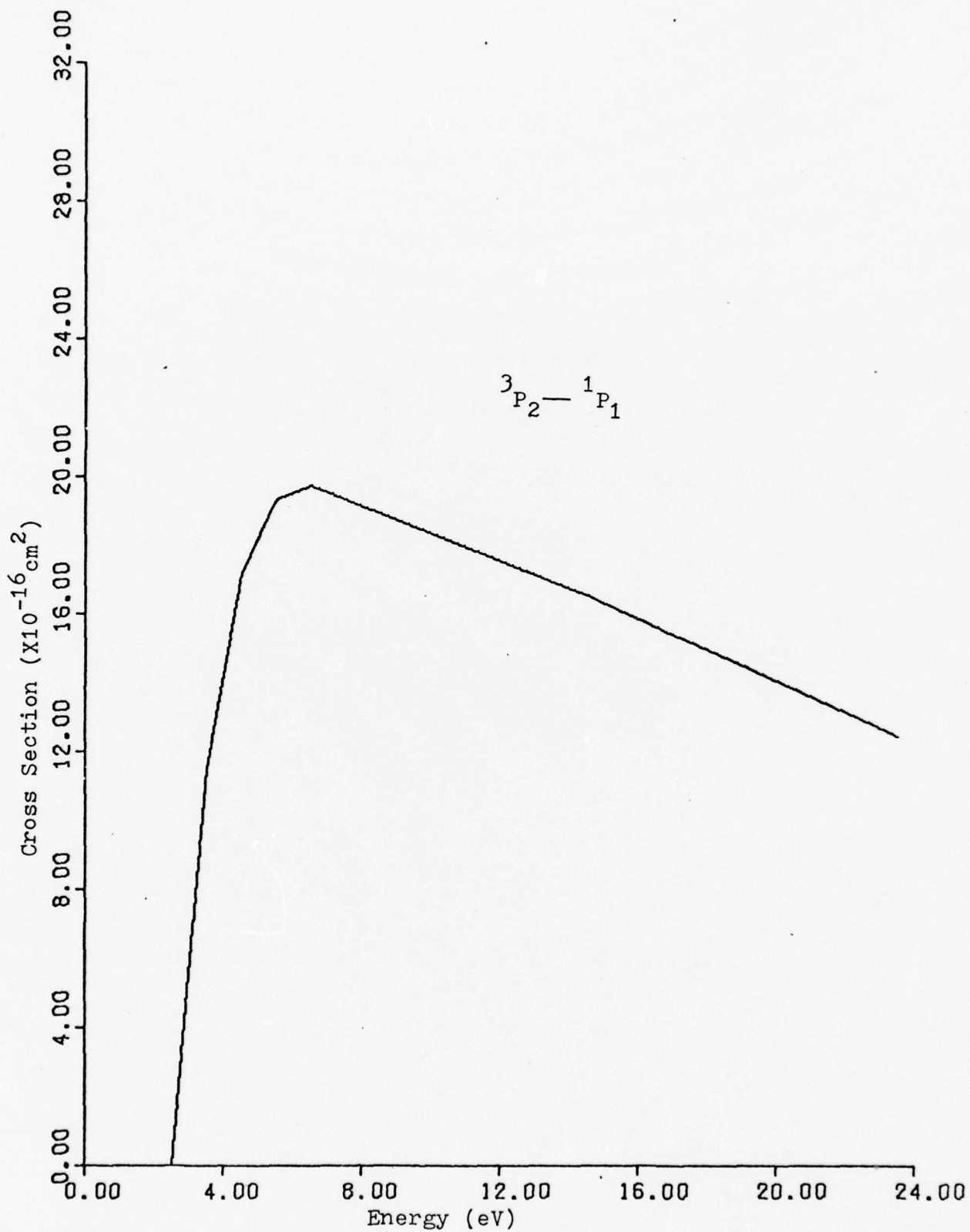


Fig. 25. Excitation of Argon by electron impact.

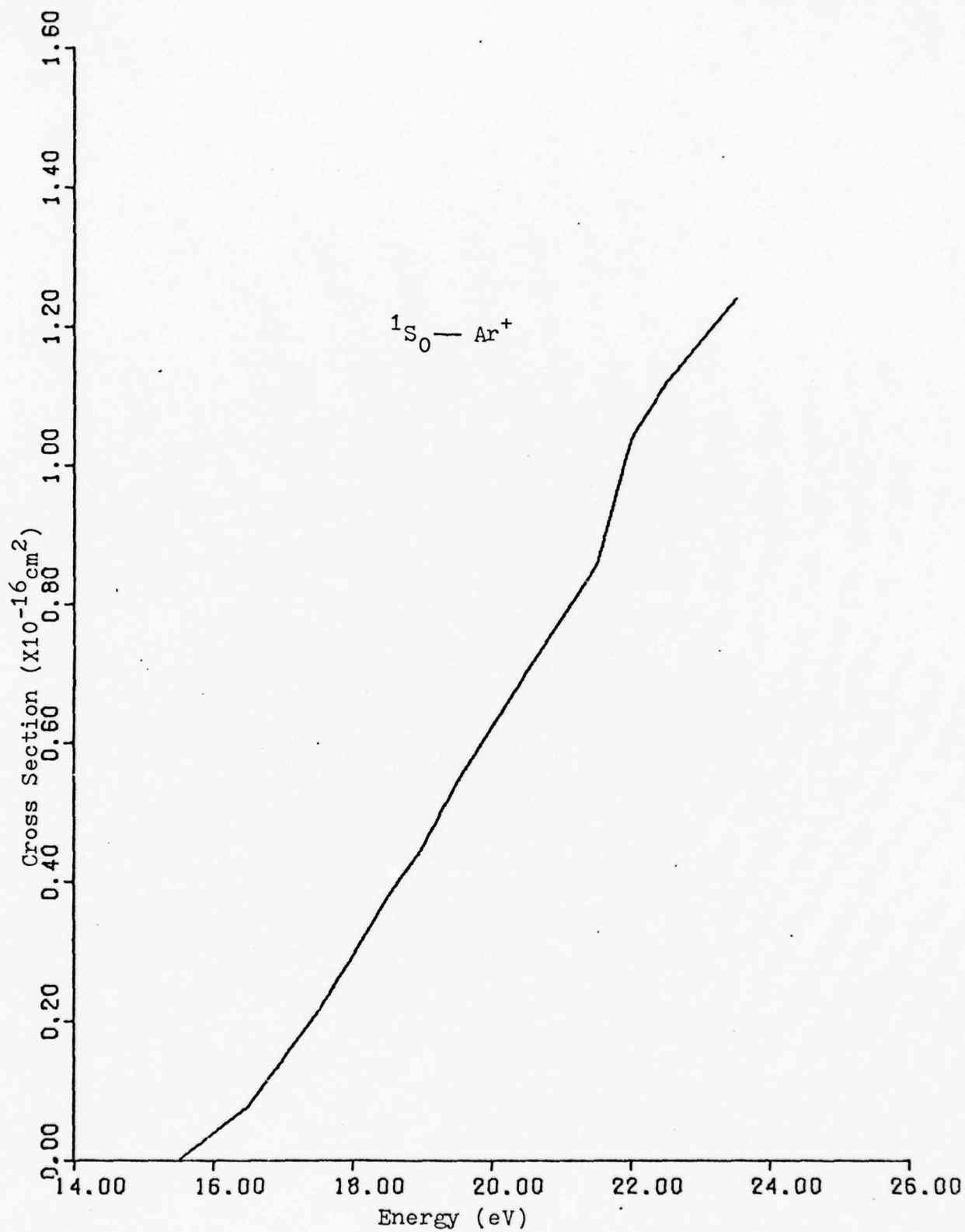


Fig. 26. Ionization of Argon by electron impact.

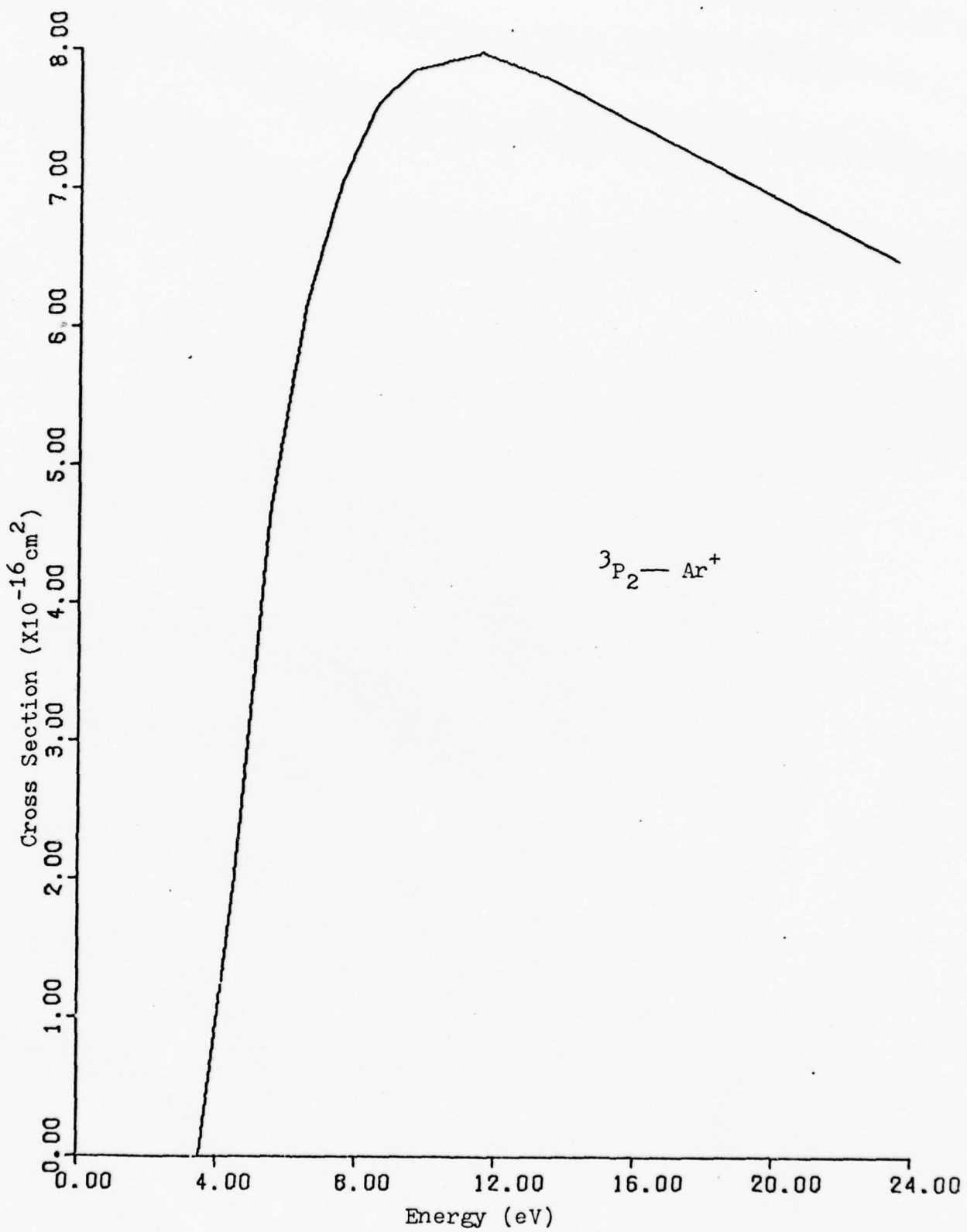


Fig. 27. Ionization of Argon by electron impact.

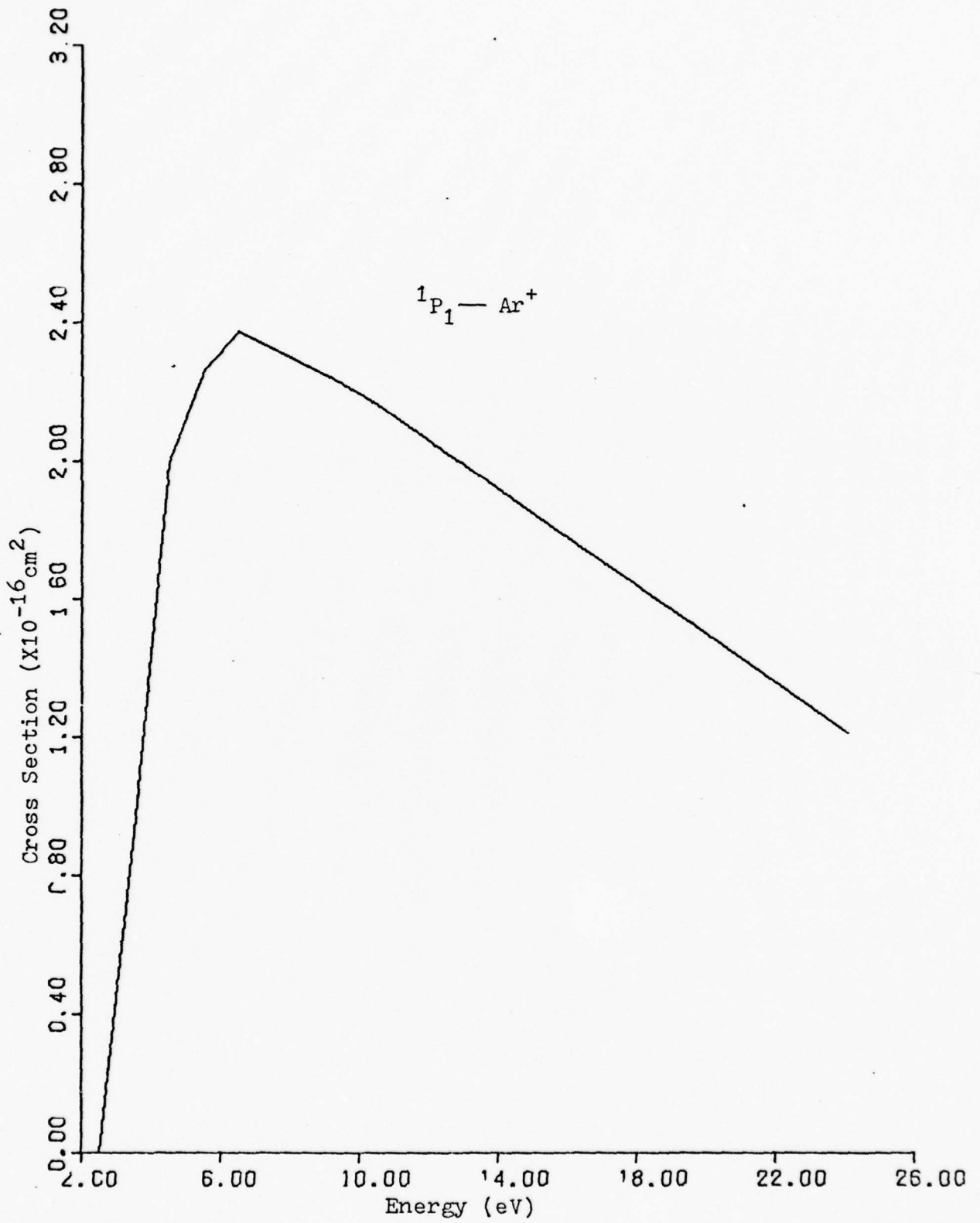


Fig. 28. Ionization of Argon by electron impact.

<u>Transition</u>	<u>Energy (eV)</u>	<u>Reference</u>	<u>Figure</u>
Ar — Ar [*]	11.7	21	23
Ar — Ar ^{**}	13.2	21	24
Ar [*] — Ar ^{**}	1.5	6	25
Ar — Ar ⁺	15.759	21	26
Ar [*] — Ar ⁺	4.059	18	27
Ar ^{**} — Ar ⁺	2.559	18	28

Chlorine (Cl₂)

The dissociative attachment rate for Cl₂ is determined by treating the cross section as a narrow function of low energy. The value of this function is $9 \times 10^{-17} \text{ cm}^2$ around zero energy and zero everywhere else. This technique is supplied by Hunter (Ref 21).

Conclusion

The results accumulated in this chapter are as complete a list as can be found. Several of the cross section values have been determined to be very accurate, while others vary up to a factor of 9 in comparison with the same cross section determined by some other means.

The lists are not meant to be complete. Their intention is to give an order-of-magnitude figure for determining the temporal evolution of the HgCl discharge. When experimental data becomes available, they should be updated with this new information.

IV. The HgCl Model

Overview

In this chapter, the discharge analysis of the HgCl laser is continued from the work initiated by Summers (Ref 4). The chapter is divided into three sections. First, an introduction to the reactions, second, a simple analytic approach, and third, a discussion of results from a complete numerical solution of the HgCl discharge.

Introduction

In order to build larger scale lasers, one must develop a comprehensive model that explicitly accounts for all significant processes. Summers (Ref 4) recognizes this need and identified many of the energy flow pathways. He also points out that two of his assumptions would need some modification. First, the assumption that the secondary electrons behave as a Maxwellian distribution, and second, that the electron beam ionization cross section for producing secondary electrons is not a function of energy.

The first assumption is eliminated by the numerical solution to the electron Boltzmann equation identified in Chapter I. The second assumption is adjusted with a technique developed by Green and Sowada (Ref 22).

The particular species which control the processes in the HgCl laser are electrons, the ground and metastable

levels of Hg, the ground and metastable levels of Ar, and the Cl₂ molecule. The continuity equations of the dominant discharge species are based on the processes listed in Table III. The table is neither complete nor does it represent a closed system of reactions. Equation numbers identified with each reaction, and typical values of reaction rate constants determined by the numerical code, are listed in Table III.

Table III
Processes Included in Discharge Model

<u>Reactions</u>	<u>Rate/Cross Section</u>	<u>Reference</u>
e-beam ionization		
$e^P + Ar \rightarrow Ar^+ + e + e^P$	$\sigma_1 = 7.68 \times 10^{-18} \text{ cm}^2$	23 (23)
$e^P + Hg \rightarrow Hg^+ + e + e^P$	$\sigma_2 = 8.17 \times 10^{-18} \text{ cm}^2$	22 (24)
electron loss		
$e + Ar_2^+ \rightarrow Ar^* + Ar$	$R_1 = 3.9 \times 10^{-8} \text{ cm}^3/\text{sec}$	4 (25)
$e + Cl_2 \rightarrow Cl^- + Cl$	$R_2 = 1.0 \times 10^{-10} \text{ cm}^3/\text{sec}$	Code (26)
$e + Hg_2^+ \rightarrow Hg^{**} + Hg$	$R_3 = 1.0 \times 10^{-7} \text{ cm}^3/\text{sec}$	11 (27)
metastable formation		
$e + Ar \rightarrow Ar^* + e$	$R_4 = 1.0 \times 10^{-12} \text{ cm}^3/\text{sec}$	Code (28)
$e + Ar^* \rightarrow Ar + e$	$R_5 = 1.0 \times 10^{-8} \text{ cm}^3/\text{sec}$	Code (29)
$e + Ar \rightarrow Ar^{**} + e$	$R_6 = 1.0 \times 10^{-12} \text{ cm}^3/\text{sec}$	Code (30)
$e + Ar^{**} \rightarrow Ar + e$	$R_7 = 1.0 \times 10^{-8} \text{ cm}^3/\text{sec}$	Code (31)
$e + Ar^* \rightarrow Ar^{**} + e$	$R_8 = 1.0 \times 10^{-7} \text{ cm}^3/\text{sec}$	Code (32)
$e + Ar^{**} \rightarrow Ar^* + e$	$R_9 = 1.0 \times 10^{-6} \text{ cm}^3/\text{sec}$	Code (33)

Table III (Cont'd)

<u>Reactions</u>	<u>Rate/Cross Section</u>	<u>Reference</u>
metastable formation		
$e + \text{Hg} \rightarrow \text{Hg}^* + e$	$R_{10} = 1.0 \times 10^{-9} \text{cm}^3/\text{sec}$	Code (34)
$e + \text{Hg}^* \rightarrow \text{Hg} + e$	$R_{11} = 1.0 \times 10^{-8} \text{cm}^3/\text{sec}$	Code (35)
$e + \text{Hg} \rightarrow \text{Hg}^{**} + e$	$R_{12} = 1.0 \times 10^{-9} \text{cm}^3/\text{sec}$	Code (36)
$e + \text{Hg}^{**} \rightarrow \text{Hg} + e$	$R_{13} = 1.0 \times 10^{-8} \text{cm}^3/\text{sec}$	Code (37)
$e + \text{Hg} \rightarrow \text{Hg}^{***} + e$	$R_{14} = 1.0 \times 10^{-10} \text{cm}^3/\text{sec}$	Code (38)
$e + \text{Hg}^{***} \rightarrow \text{Hg} + e$	$R_{15} = 1.0 \times 10^{-8} \text{cm}^3/\text{sec}$	Code (39)
$e + \text{Hg} \rightarrow \text{Hg}^{****} + e$	$R_{16} = 1.0 \times 10^{-10} \text{cm}^3/\text{sec}$	Code (40)
$e + \text{Hg}^{****} \rightarrow \text{Hg} + e$	$R_{17} = 1.0 \times 10^{-8} \text{cm}^3/\text{sec}$	Code (41)
$e + \text{Hg}^* \rightarrow \text{Hg}^{**} + e$	$R_{18} = 1.0 \times 10^{-8} \text{cm}^3/\text{sec}$	Code (42)
$e + \text{Hg}^{**} \rightarrow \text{Hg}^* + e$	$R_{19} = 1.0 \times 10^{-7} \text{cm}^3/\text{sec}$	Code (43)
$e + \text{Hg}^* \rightarrow \text{Hg}^{***} + e$	$R_{20} = 1.0 \times 10^{-10} \text{cm}^3/\text{sec}$	Code (44)
$e + \text{Hg}^{***} \rightarrow \text{Hg}^* + e$	$R_{21} = 1.0 \times 10^{-8} \text{cm}^3/\text{sec}$	Code (45)
$e + \text{Hg}^* \rightarrow \text{Hg}^{****} + e$	$R_{22} = 1.0 \times 10^{-11} \text{cm}^3/\text{sec}$	Code (46)
$e + \text{Hg}^{****} \rightarrow \text{Hg}^* + e$	$R_{23} = 1.0 \times 10^{-9} \text{cm}^3/\text{sec}$	Code (47)
$e + \text{Hg}^{**} \rightarrow \text{Hg}^{***} + e$	$R_{24} = 1.0 \times 10^{-10} \text{cm}^3/\text{sec}$	Code (48)
$e + \text{Hg}^{***} \rightarrow \text{Hg}^{**} + e$	$R_{25} = 1.0 \times 10^{-8} \text{cm}^3/\text{sec}$	Code (49)
$e + \text{Hg}^{**} \rightarrow \text{Hg}^{****} + e$	$R_{26} = 1.0 \times 10^{-8} \text{cm}^3/\text{sec}$	Code (50)
$e + \text{Hg}^{****} \rightarrow \text{Hg}^{**} + e$	$R_{27} = 1.0 \times 10^{-7} \text{cm}^3/\text{sec}$	Code (51)
$e + \text{Hg}^{***} \rightarrow \text{Hg}^{****} + e$	$R_{28} = 1.0 \times 10^{-7} \text{cm}^3/\text{sec}$	Code (52)
$e + \text{Hg}^{****} \rightarrow \text{Hg}^{***} + e$	$R_{29} = 1.0 \times 10^{-7} \text{cm}^3/\text{sec}$	Code (53)
ionization formation		
$e + \text{Ar} \rightarrow \text{Ar}^+ + 2e$	$R_{30} = 1.0 \times 10^{-15} \text{cm}^3/\text{sec}$	Code (54)
$e + \text{Ar}^* \rightarrow \text{Ar}^+ + 2e$	$R_{31} = 1.0 \times 10^{-8} \text{cm}^3/\text{sec}$	Code (55)

Table III (Cont'd)

<u>Reactions</u>	<u>Rate/Cross Section</u>	<u>Reference</u>
ionization formation		
$e + \text{Ar}^{**} \rightarrow \text{Ar}^+ + 2e$	$R_{32} = 1.0 \times 10^{-7} \text{cm}^3/\text{sec}$	Code (56)
$e + \text{Hg} \rightarrow \text{Hg}^+ + 2e$	$R_{33} = 1.0 \times 10^{-11} \text{cm}^3/\text{sec}$	Code (57)
$e + \text{Hg}^* \rightarrow \text{Hg}^+ + 2e$	$R_{34} = 1.0 \times 10^{-8} \text{cm}^3/\text{sec}$	Code (58)
$e + \text{Hg}^{**} \rightarrow \text{Hg}^+ + 2e$	$R_{35} = 1.0 \times 10^{-8} \text{cm}^3/\text{sec}$	Code (59)
$e + \text{Hg}^{***} \rightarrow \text{Hg}^+ + 2e$	$R_{36} = 1.0 \times 10^{-7} \text{cm}^3/\text{sec}$	Code (60)
$e + \text{Hg}^{****} \rightarrow \text{Hg}^+ + 2e$	$R_{37} = 1.0 \times 10^{-6} \text{cm}^3/\text{sec}$	Code (61)
excimer formation		
$\text{Hg}^+ + \text{Cl} \rightarrow \text{HgCl}^*$	$R_{38} = 1.0 \times 10^{-6} \text{cm}^3/\text{sec}$	4 (62)
$\text{Hg}^* + \text{Cl}_2 \rightarrow \text{HgCl}^* + \text{Cl}$	$R_{39} = 3.8 \times 10^{-10} \text{cm}^3/\text{sec}$	11 (63)
$\text{Hg}^{**} + \text{Cl}_2 \rightarrow \text{HgCl}^* + \text{Cl}$	$R_{40} = 2.0 \times 10^{-11} \text{cm}^3/\text{sec}$	11 (64)
$\text{Hg}^{***} + \text{Cl}_2 \rightarrow \text{HgCl}^* + \text{Cl}$	$R_{41} = 4.0 \times 10^{-10} \text{cm}^3/\text{sec}$	11 (65)
$\text{Hg}^{****} + \text{Cl}_2 \rightarrow \text{HgCl}^* + \text{Cl}$	$R_{42} = 4.0 \times 10^{-10} \text{cm}^3/\text{sec}$	11 (66)
$\text{Hg}_2^+ + \text{Cl} \rightarrow \text{HgCl}^* + \text{Hg}$	$R_{43} = 1.0 \times 10^{-6} \text{cm}^3/\text{sec}$	11 (67)
$\text{Ar}^+ + \text{Cl} \rightarrow \text{ArCl}^*$	$R_{44} = 2.13 \times 10^{-6} \text{cm}^3/\text{sec}$	4 (68)
$\text{Ar}^* + \text{Cl}_2 \rightarrow \text{ArCl}^* + \text{Cl}$	$R_{45} = 3.16 \times 10^{-10} \text{cm}^3/\text{sec}$	4 (69)
excimer loss		
$\text{HgCl}^* \rightarrow \text{HgCl} + h\nu$	$R_{46} = 2.2 \times 10^7/\text{sec}$	11 (70)
$\text{HgCl}^* + \text{Cl}_2 \rightarrow \text{Quench}$	$R_{47} = 4.6 \times 10^{-10} \text{cm}^3/\text{sec}$	11 (71)
$\text{HgCl}^* + \text{Ar} \rightarrow \text{Quench}$	$R_{48} = 9.0 \times 10^{-14} \text{cm}^3/\text{sec}$	11 (72)
$\text{HgCl}^* + \text{Hg} \rightarrow 2\text{Hg} + \text{Cl}$	$R_{49} = 1.0 \times 10^{-10} \text{cm}^3/\text{sec}$	11 (73)
$\text{ArCl}^* \rightarrow \text{Ar} + \text{Cl} + h\nu$	$R_{50} = 5.0 \times 10^7/\text{sec}$	4 (74)

Table III (Cont'd)

<u>Reactions</u>	<u>Rate/Cross Section</u>	<u>Reference</u>
3 body reactions		
$\text{Ar}^+ + 2\text{Ar} \rightarrow \text{Ar}_2^+ + \text{Ar}$	$R_{51} = 2.5 \times 10^{-31} \text{cm}^6/\text{sec}$	4 (75)
$\text{Cl} + \text{Cl} + \text{Cl}_2 \rightarrow 2\text{Cl}_2$	$R_{52} = 1.165 \times 10^{-32} \text{cm}^6/\text{sec}$	4 (76)
$\text{Cl} + \text{Cl} + \text{Ar} \rightarrow \text{Cl}_2 + \text{Ar}$	$R_{53} = 1.957 \times 10^{-32} \text{cm}^6/\text{sec}$	4 (77)
$\text{Hg}^+ + \text{Hg} + \text{Ar} \rightarrow \text{Hg}_2^+ + \text{Ar}$	$R_{54} = 1.0 \times 10^{-31} \text{cm}^6/\text{sec}$	11 (78)
$\text{Hg} + \text{Cl} + \text{Ar} \rightarrow \text{HgCl} + \text{Ar}$	$R_{55} = 7.5 \times 10^{-31} \text{cm}^6/\text{sec}$	11 (79)
lower level loss		
$2\text{HgCl} \rightarrow \text{Hg} + \text{HgCl}_2$	$R_{56} = 3.0 \times 10^{-10} \text{cm}^3/\text{sec}$	11 (80)
$2\text{HgCl} \rightarrow \text{Hg}_2\text{Cl}_2$	$R_{57} = 2.0 \times 10^{-10} \text{cm}^3/\text{sec}$	11 (81)
$\text{HgCl} + \text{Cl}_2 \rightarrow \text{HgCl}_2 + \text{Cl}$	$R_{58} = 1.0 \times 10^{-11} \text{cm}^3/\text{sec}$	11 (82)
Penning Ionization		
$\text{Hg} + \text{Ar}^+ + \text{Ar} + e + \text{Hg}^+$	$R_{59} = 4.37 \times 10^{-12} \text{cm}^3/\text{sec}$	Cal (83)
metastable transfer		
$\text{Hg}^{****} + \text{Ar} \rightarrow \text{Hg}^{***} + \text{Ar}$	$R_{60} = 1.0 \times 10^{-13} \text{cm}^3/\text{sec}$	11 (84)
$\text{Hg}^{***} + \text{Ar} \rightarrow \text{Hg}^{**} + \text{Ar}$	$R_{61} = 1.0 \times 10^{-14} \text{cm}^3/\text{sec}$	11 (85)

Rate constants identified by Tang (Ref 11) in Table III are reasonably accurate though uncertainties of ~50% are possible. Reaction rate constants calculated by the code are accurate to an order of magnitude.

In Table III, the reference to code indicates this reaction rate constant is dependent upon parameters placed on the discharge. Values of these rates are calculated by

the numerical solution of Chapter I and are not listed here. The cross sections for electron beam ionization, reactions 23 and 24, and the calculation of Penning ionization, reaction 83, are calculated in Appendix B. The quenching products of reactions 71 and 72 are considered insignificant to the overall gas discharge.

Table III is as complete a table of reactions as can be found. Any reaction omitted is due to either the non-availability of cross section information or the reaction is thought to be insignificant to the overall process.

In the next section, a simple discharge analysis is developed. The purpose of the section is to illustrate the physical character of the processes taking place. For simplicity, only a few of the reactions of Table III are used.

Theory

General Reactions. A rate equation can be generalized as equation 86 where n_i is the number density of species i .

$$\dot{n}_i = \Sigma \left(\begin{array}{l} \text{all processes} \\ \text{creating } n_i \end{array} \right) - \Sigma \left(\begin{array}{l} \text{all processes} \\ \text{annihilating } n_i \end{array} \right) \quad (86)$$

A simple example of some of these processes is shown in equation 87, where i represents the upper laser level.

$$\begin{aligned} \dot{n}_i = & \left(\begin{array}{l} \text{electron impact} \\ \text{pumping} \end{array} \right) + \left(\begin{array}{l} \text{chemical} \\ \text{pumping} \end{array} \right) \\ & - \left(\begin{array}{l} \text{stimulated} \\ \text{emission} \end{array} \right) - \left(\begin{array}{l} \text{spontaneous} \\ \text{emission} \end{array} \right) \end{aligned} \quad (87)$$

In equation 87, the term electron impact processes are those processes which create or destroy metastable levels by collisions of the first or second kind (Ref 24). The term stimulated emission deals with optical excitation and deexcitation, while the term spontaneous emission is the process of radiative relaxation. A full understanding of the chemical pumping term is beyond the scope of this paper.

The next section is the development of the discharge analysis. A complete analysis is virtually impossible, therefore, reactions that characterize the overall physics of the process are used.

Model

The rate equations 88 through 90 are assumed to be the controlling processes in the HgCl discharge evolution.

Electrons

$$\dot{n}_e = S_1 - R_2 n_e n_{Cl_2} + R_{33} n_e n_{Hg} + R_{34} n_e n_{Hg}^* \quad (88)$$

Hg*

$$\begin{aligned} \dot{n}_{Hg}^* = & R_{10} n_e n_{Hg} - R_{11} n_e n_{Hg}^* + R_{19} n_e n_{Hg}^{**} \\ & - R_{34} n_e n_{Hg}^* - R_{39} n_{Hg}^* n_{Cl_2} - R_{18} n_e n_{Hg}^* \end{aligned} \quad (89)$$

Cl₂

$$\dot{n}_{Cl_2} = - R_2 n_e n_{Cl_2} - R_{39} n_{Hg}^* n_{Cl_2} \quad (90)$$

In equation 88, S_1 is a source term of secondary electrons generated from the electron beam. A development of these source terms is explained in Appendix B. Each term in equations 89 through 90 represents a different reaction of Table III. The reaction process for each of these terms is identified with the appropriate rate symbol.

Equations 89 through 90 can be solved to determine both the temporal evolution of the discharge, and the conditions for the existence of steady-state solutions. Once the conditions are determined, a study of the stability can be made.

The rate equation for the electron number density, equation 88, is determined by a balance between ionization rates and electron attachment rates. Steady state operation is never quite achieved because the electron number density increases as the rate of dissociative attachment, equation 90, decreases.

Summers (Ref 4) identified two important points that aid in the analysis. First, the depletion of Cl_2 is slower than the rate of ionization of Hg by at least an order-of-magnitude. Second, the ground state neutral species vary on time scales of microseconds while ionized species vary on the order of nanoseconds. Because of these features, equilibrium can be reached on short time scales even though long term equilibrium is impossible.

The equilibrium of metastable species, equation 89, can be controlled by either a dominant eximer formation or

by a dominant ionization of metastable levels. It is of interest to examine both of these conditions.

When excimer formation is dominant, equation 89 becomes equation 91.

$$n_{\text{Hg}^*} \sim \frac{R_{10} n_e n_{\text{Hg}}}{R_{39} n_{\text{Cl}_2}} \quad (91)$$

The electron rate equation now becomes equation 92.

$$\dot{n}_e = S_1 + n_e [R_{33} n_{\text{Hg}} - R_2 n_{\text{Cl}_2}] + n_e^2 [\frac{R_{35} R_{10} n_{\text{Hg}}}{n_{\text{Cl}_2}}] \quad (92)$$

In equilibrium, $\dot{n}_e = 0$, the electron number density is determined by solving the quadratic. The time dependent solution is obtained by direct integration.

Fortunately, Hunter (Ref 21) has already evaluated a similar function with the KrF_2 laser. He shows that the excimer formation equilibrium is a condition corresponding to an electron beam dominated discharge.

If the electron density becomes large enough for metastable loss rates to be dominated by ionization, equation 89 becomes equation 93.

$$n_{\text{Hg}^*} \sim \frac{R_{10} n_e n_{\text{Hg}}}{R_{34} n_e} = \frac{R_{10} n_{\text{Hg}}}{R_{34}} \quad (93)$$

The electron density rate equation is now approximated by equation 94.

$$\dot{n}_e = S_1 - n_e [R_2 n_{Cl_2} - R_{33} n_{Hg^+}] + n_e [\frac{R_{10} n_{Hg}}{R_{34}}] \quad (94)$$

or

$$\dot{n}_e = S_1 + \gamma n_e \quad (95)$$

In equation 95, γ is the electron attachment rate minus the cumulative ionization rate.

The time dependent solution is found by integration, and the equilibrium condition is simply

$$n_e = \frac{S_1}{\gamma} \quad (96)$$

Hunter (Ref 21) also shows that this equilibrium corresponds to a field-dominated discharge. His results are shown in Figure 29.

The temporal evolution of the discharge varies according to the concentration of Cl_2 and Hg. If the eximer formation equilibrium is obtained, the depletion of Cl_2 will cause the discharge to transition to ionization equilibrium. This is caused by the continual depletion of Cl_2 by dissociative attachment. Once the electrons reach a certain density, the depletion of Cl_2 rapidly increases by the increasing secondary electron density and breakdown is forthcoming. The production of electrons in the ionization

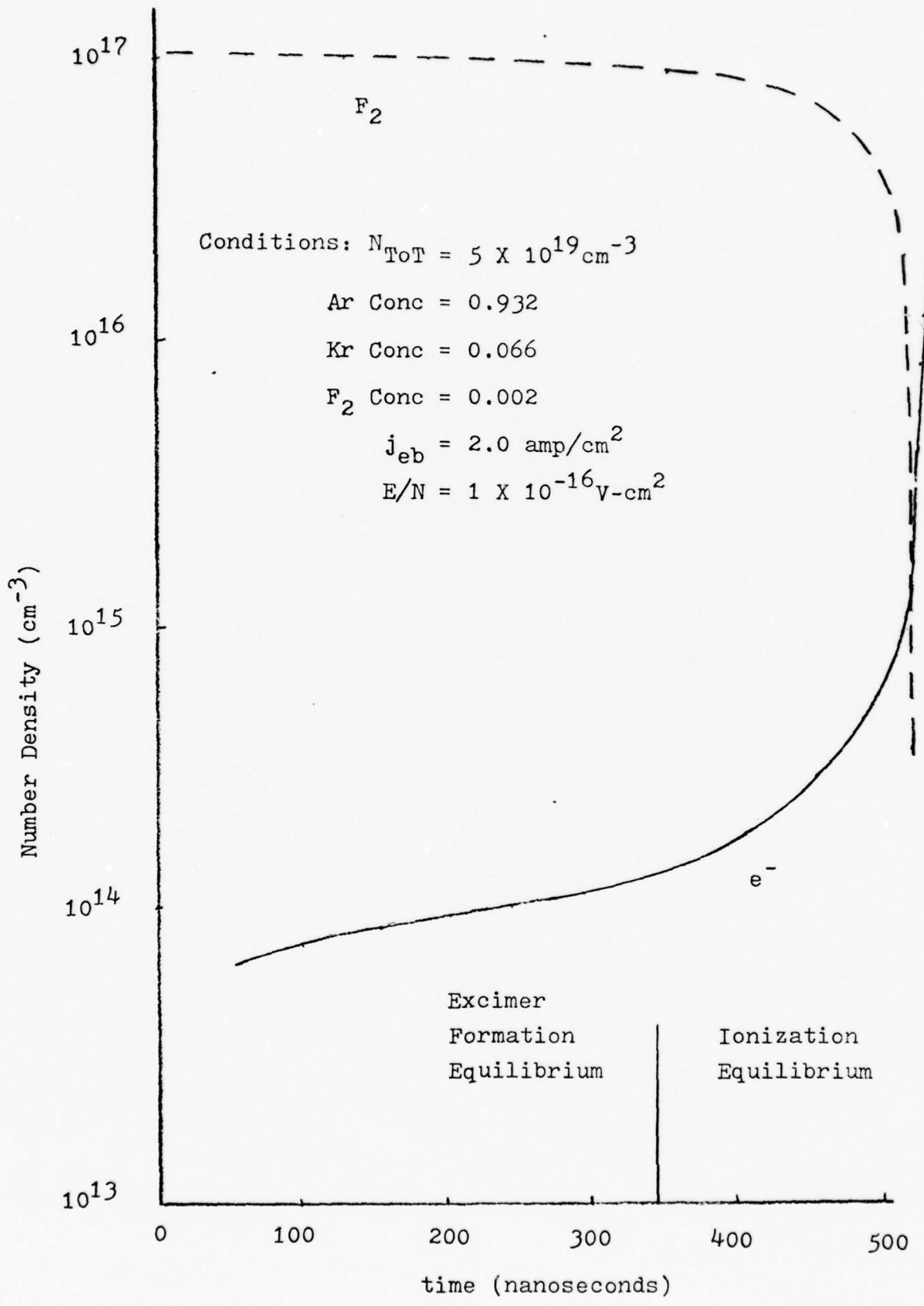


Fig. 29 Temporal evolution of KrF discharge(Ref 21).

equilibrium region is approximately equal to the number density of ionized mercury because of its low ionization energy.

Intensity

Another interesting feature to evaluate is the intensity rate of the laser discharge. The stimulated emission term of equation 87 can be rewritten as equation 97 (Ref 26).

$$\Delta n = \sigma n \left(N_u - \frac{g_u}{g_l} N_l \right) \quad (97)$$

In equation 97, the subscripts u and l represent the upper and lower laser levels, respectively. The N represents the number density of the appropriate level, and n is the photon flux in $\text{cm}^{-2}\text{sec}^{-1}$. The symbol g stands for the degeneracy of that state, while the symbol σ is the stimulated cross section shown in equation 98 (Ref 26).

$$\sigma = \frac{\lambda^4}{8\pi^2 \tau c \delta \lambda} \quad (98)$$

where λ is the wavelength in cm

τ is the Einstein A^{-1} coefficient

c equals the speed of light in cm/sec

$\delta \lambda$ is the half width of half max

Assuming the degeneracies of the upper and lower level to be equal, the gain of the medium is simply equation 99.

$$g = \sigma [N_u - N_l] \quad (99)$$

In general, the change in intensity of a laser medium is shown in equation 100 (Ref 25).

$$\dot{I} = cI (g - g_{th}) \quad (100)$$

where g_{th} represents the laser threshold gain. Hunter (Ref 21) derives a more complete intensity equation, which include, a term due to the spontaneous radiation. This is shown in equation 101.

$$\dot{I} = cI (g - g_{th}) + \frac{ch\nu N_u d\Omega}{4\pi\tau} \text{spontaneous} \quad (101)$$

In equation 101, $h\nu$ is the energy of the photon, $d\Omega$ the solid angle based on the length of the cavity, and τ the inverse Einstein A coefficient.

The next section discusses the results generated from the numerical solution of the HgCl laser.

Discussion

It is interesting to note some of the results of the numerical solution. The time to breakdown is very sensitive to the concentration of Hg. With a very small field, 1 Townsend or less, a beam of 1 amp/cm² caused breakdown

inside of 100 nanoseconds, with a ratio of Ar/Hg/Cl₂ as 95%/95%/4.8%/0.2%. Reducing the concentrations to match those of Tang (Ref 1), breakdown occurred in a much longer time period. The sensitivity of breakdown to Cl₂ is expected since this is the only "sink" term for electrons.

It is also interesting to note that the addition or removal of the "stored energy" levels of the mercury atom, did not significantly effect the temporal evolution of the discharge.

V. Results and Recommendations

Results

The purpose of this paper is to determine the temporal evolution of the HgCl discharge. It has reached that objective. Before presenting the results, a few words about the concluding remarks are apropos.

It is always easiest to arrive at a conclusion when there are experimental data to back the results. In the case of the HgCl laser, there aren't many experimental data, but there is enough to give credibility to any matching numerical solution.

The results of this paper are determined more from basic physics, and knowing a "ball park" figure, than from any great esoteric derivation. They are by no means an attempt to discredit any published literature. There are three results that point out areas that need more research in order to better model the HgCl laser.

First, a complete numerical solution of the electron Boltzmann equation was determined. This numerical solution was checked against two sources of information and agreed remarkably well.

When fractional energy deposition was compared to Rockwood (Ref 5), a definite difference was noted in the lower E/N values (Figure 2). Rockwood observed a bend in this region, while the results of the numerical solution

used in this paper did not match those results. This was first thought to be the effect of a coarse bin width of 1 eV. After including elastic collisions, it was determined that the bend was the result of elastic processes dominating the discharge. The original assumption of considering elastic collision processes to be insignificant had to be abandoned if results were to be reliable in all ranges of E/N .

Second, the cross sections for transitions among metastable levels of Hg are calculated with tested known theory. There appears to be a small difference between calculated and published information on cross sections, however, a more significant point is the sensitivity of the reaction rate constants of these cross sections. Varying a cross section by an order of magnitude varies the reaction rate constant by at least an order of magnitude. It is also found that the overall discharge characteristic did not change when including the higher stored energy levels. The most significant contribution to the discharge is the ionization of the 6^3P_2 level of Mercury. As soon as this level became significantly populated ($\sim 10^{15} \text{cm}^{-3}$), breakdown occurred in a matter of nanoseconds. This is due mostly to the ionization process of the 6^3P_2 level.

Third, the temporal evolution of the HgCl laser yields results that are somewhat interesting. This third, and most significant feature, calls for some speculation on the information supplied to the numerical HgCl laser program.

On the initial runs of the HgCl laser program, secondary electron number densities were building up in a remarkably short time. With no E field on the gas and an electron beam of 1 amp/cm^2 , breakdown occurred in less than 100 nanoseconds. A figure of 400 to 500 nanoseconds is more reasonable.

The rapid buildup of secondary electrons was first thought to be the result of ignoring collisions of the second kind - it wasn't. Perhaps the idea of stored energy in the higher metastable levels of mercury over-estimated the excited number densities. This adjustment did not make an appreciable change. Finally, a reduction in the electron exchange cross sections gave the results more physical meaning. Gas breakdown did not occur up to times of 250 nanoseconds or greater. The gas reached a transient stable condition. By increasing either the electron beam or the E field, breakdown occurred in shorter time periods.

It is also evident that the concentration of mercury strongly controls the electron density. A factor of 5 reduction in the concentration increased the time to breakdown significantly.

The reactions of Table III are the ones that determine the twenty-one differential equations to be solved. The numerical solution of these differential equations yield the temporal evolution of the HgCl discharge. Although the stiffness of the differential equations prohibited the integrator from solving the equations beyond 200 nanoseconds,

a general trend can be seen as compared to the KrF discharge. This is shown in Figure 30.

Small variations in the initial concentration of Cl_2 also effect the electron build-up significantly. The concentrations were finally adjusted to match the values used by Hunter (Ref 1). In his experiment he also noted the sensitivity of the discharge to the concentration of Cl_2 . It is the above results that lead to the following recommendations.

Recommendations

In summary, work needs to be continued in three major areas. First, a closer examination of the excitation cross sections for Hg should be attempted. This can be accomplished by either redoing the work of Rockwood (Ref 5) or by attempting a quantum mechanical calculation similar to that of Yavorsky (Ref 12). Second, a determination of several other reactions, should be evaluated. This evaluation should include an examination of the lower ^3P levels of mercury. Nikitin (Ref 27) suggests that the $^3\text{P}_0$ level may become heavily populated from the higher levels of mercury. The examination should also include a means of removing the lower levels of HgCl. Burnham (Ref 28) shows a marked increase in efficiency with the addition of the diatomic molecule N_2 . Third, experimental comparison must be continued. This part can best be accomplished by finding a better integrator for the stiff differential equations.

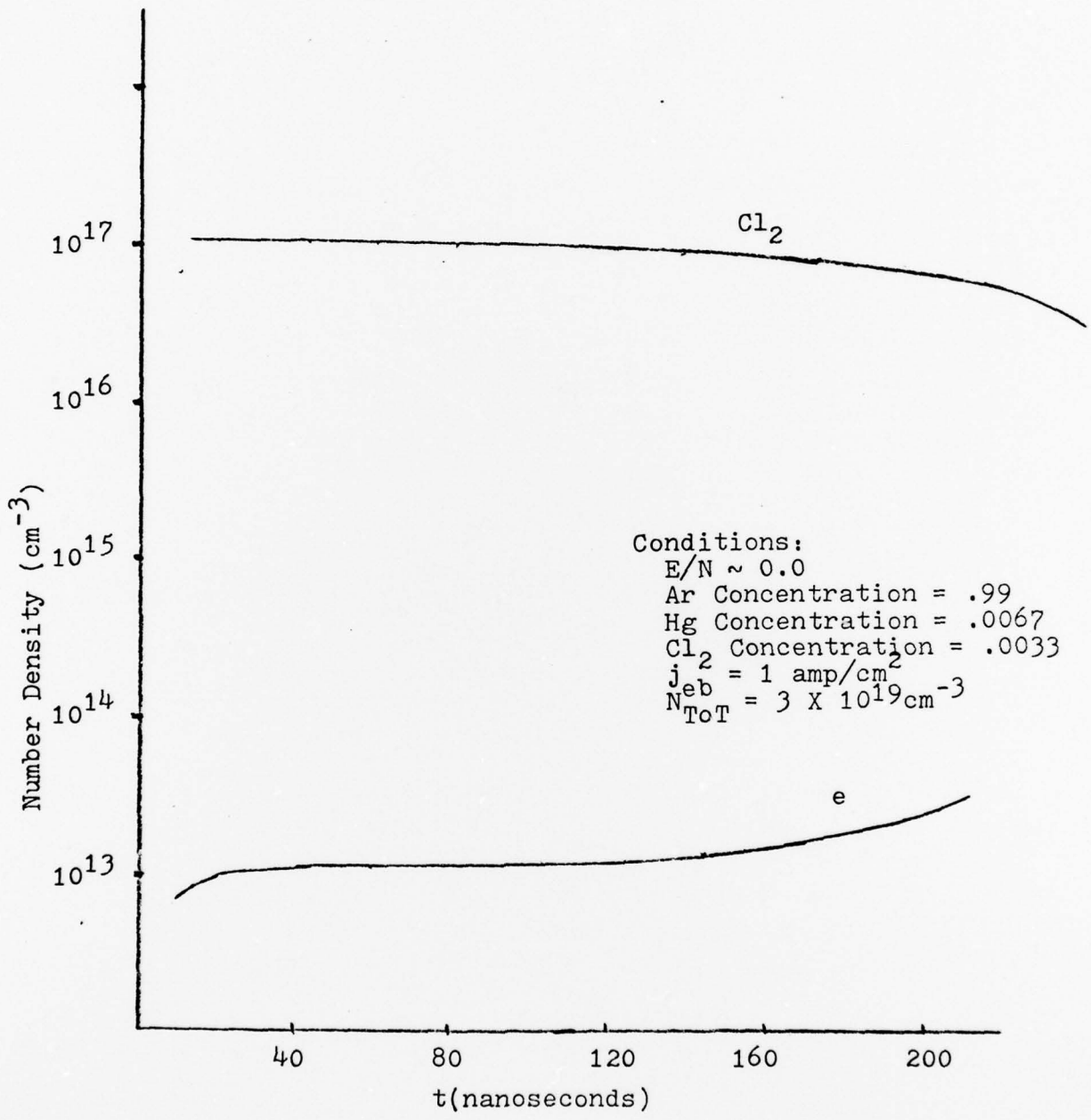


Fig. 30 Temporal Evolution of HgCl Discharge.

The HgCl laser is in the infancy of development and the pathwork for understanding a large-scale, viable laser is laid out. The gain of insight toward the microscopic processes will be invaluable in any e-beam controlled discharge laser.

References

1. K. Y. Tang, R. O. Hunter, Jr., J. Oldenettel, C. Howton, D. Huestis, D. Eckstrom, B. Perry, and M. McCusker. Appl. Phys. Lett., 32:226 (1978)
2. J. H. Parks. Appl. Phys. Lett., 31:192 (1977).
3. J. Gary Eden. Appl. Phys. Lett., 31:448 (1977).
4. R. P. Summers. "Reaction-Rate Constants and Simple Rate Theories Applied to the Mercury Chloride Laser". Unpublished Thesis, AFIT, Wright-Patterson AFB, Ohio. 1978.
5. Stephen D. Rockwood. Phys. Rev. A., 8: 2348 (1973).
6. William L. Nighan. Phys. Rev. A., 2:1989 (1970).
7. Phil Neilsen. Private Communication.
8. Gerhard Herzberg. Atomic Spectra and Atomic Structure. (Dover Publications, New York, New York, 1944) pp. 65.
9. R. J. Anderson, E. T. P. Lee, and C. C. Lin. Phys. Rev., 157:33 (1967).
10. K. Panevkin. Papers of Acad. of Sci. U.S.S.R., 59: 683 (1948).
11. K. Y. Tang. Maxwell Labs, San Diego, Ca. Private Communication.
12. B. Yavorski. J. Phys. U.S.S.R., 10:476 (1946).
13. E. Bauer and C. D. Bartkly. J. Chem. Phys., 43:2466 (1965).
14. P. Thomson, Phil. Mag., 23:449 (1912).
15. H. W. Drawin, Zeit. f. Physik., 164:513 (1961).
16. M. Gryzinski, Phys. Rev., 115:374 (1959).
17. V. I. Oshkur and A. M. Petrun'kin. Opt. Spectry., 14: 245 (1963).
18. L. Vriens. Phys. Lett., 8: 260 (1964).

19. M. A. Cayless. Brit. J. Appl. Phys., 10: 187 (1959).
20. Alan Garscaddan. WPAFB, Dayton, OH. Private Communication.
21. A. Hunter. WPAFB, Dayton, OH. Private Communication.
22. A. E. S. Green and T. Sawada. J. Atmos. Terr. Phys., 34: 1719 (1972). -
23. J. N. Bass, R. A. Berg, and A. E. S. Green. J. Phys. B, 1: 1853 (1974).
24. F. K. Richtmyer, E. H. Kennard, and T. Lauritsen. Introduction to Modern Physics, (McGraw-Hill Company, New York, 1955), p. 166.
25. A. E. Siegman. An Introduction To Lasers and Masers. (McGraw-Hill Co., New York, New York, 1971), P. 402.
26. Stanford Research Institute Report NO. MP78-07, (Stanford Research Institute, Menlo Park, California, May 1978).
27. E. E. Nikitin. Theory of Elementary Atomic and Molecular Processes in Gases. (Clarendon Press, Oxford, England, 1974) p. 161.
28. R. Burnham. Appl. Phys. Lett., 33: 156 (1978).
29. M. Stamm, and P. Bailey. Private Communication.
30. A. V. Phelps and J. P. Molnar. Phys. Rev., 89: 1202-1208 (1953).

APPENDIX A

Transfers among the $6^3P_{2,1,0}$ states are not widely known. Yavorsky (Ref 12) calculates the $6^3P_1 - 6^3P_2$ transition with the result shown in Figure 31.

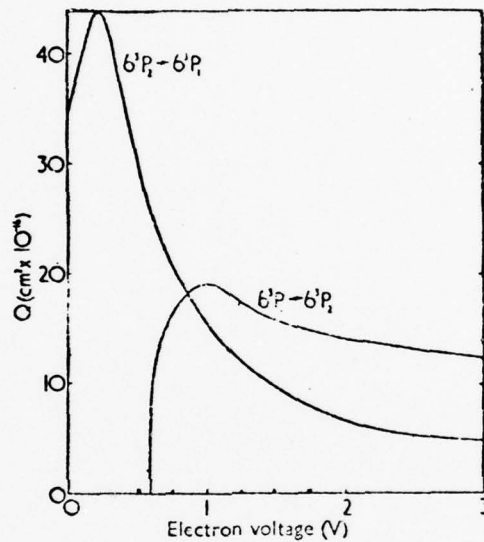


Fig. 31. Cross-sections for transitions of the first and second kind between 6^3P_1 and 6^3P_2 , after Yavorski.

Unfortunately no data on the other transitions exists. Cayless (Ref 19) uses a simple Boltzmann population argument to show that the cross sections for excitation from $o e^3P$ state to another does not differ greatly from one another.

APPENDIX B

Penning Ionization

The reaction 83 of $4.37 \times 10^{-12} \text{ cm}^3/\text{sec}$ is determined by the equation

$$R = \langle \sigma v \rangle = \frac{\int_0^{\infty} \frac{2}{m} \sigma(\epsilon) \epsilon^{1/2} f(\epsilon) d\epsilon}{\int_0^{\infty} f(\epsilon) d\epsilon} \quad (1)$$

where ϵ is energy (eV), σ is cross section (cm^2) and $f(\epsilon)$ is the number of atoms per cm^3 per eV. Assuming the distribution of heavy species ($\text{Hg} + \text{Ar}^*$) are in a Maxwellian Distribution equation (1) becomes equation (2)

$$R = \sigma v = \sigma \left(\frac{8kT}{\pi M_r} \right)^{1/2}, \quad M_r = \frac{M_1 M_2}{M_1 + M_2} \quad (2)$$

$T = 300^\circ\text{K}$ $K = \text{Boltzmann constant}$

$M_1 = 200.59 \text{ AMU (Hg)}$

$M_2 = 39.95 \text{ AMU (Ar)}$

Using the cross section determined by Phelps (Ref 30) of $1 \times 10^{-14} \text{ cm}^2$ for Penning ionization results in

$$R = 4.37 \times 10^{-12} \text{ cm}^3/\text{sec}$$

e-beam ionization

The approach used in calculating the reaction rate constant is the one utilized by Green and Sawada (Ref 22) and by Bass, Berg, and Green (Ref 23).

$$S(E,T) = A(E) \frac{\Gamma(E)^2}{[T-T_0(E)]^2 + \Gamma(E)^2} \quad (1)$$

where

$$A(E) = 10^{-16} \text{cm}^2 \frac{\text{K}}{\text{E}} \ln \left(\frac{\text{E}}{\text{J}} \right) ,$$

$$\Gamma(E) = \Gamma_s \frac{E}{E + \Gamma_b} \quad , \quad T_0(E) = T_s - \frac{T_a}{E + T_b}$$

and the units of $S(E,T)$ are cm^2/eV .

$$\sigma = \int S(E,T) dT = \text{total ionization cross section} \quad (2)$$

$$\sigma = A(E) (E) \left[\tan^{-1} \left(\frac{t_m - t_0}{\Gamma} \right) + \tan^{-1} \left(\frac{T_0}{\Gamma} \right) \right] ,$$

where $T_m = \frac{1}{2} (E-I)$

The parameters used for Hg are those of Smith-Liska in Ref 23, while those for Ar are the ones listed in Ref 22. An Energy (ϵ) of 300KeV is used for the electron energy. The units of $S(E,T)$ and T_m are cm^2/eV and eV respectively.

APPENDIX C

Numerical Code

The numerical solution of the Boltzmann time-dependent equation is the joint effort of several people. By projecting the equation on an energy axis of K bins with width $\Delta\epsilon$, the result is a set of K coupled differential equations. The form of these equations can be put in the following notation (Ref 5).

$$\begin{aligned} \dot{n}_k = & - \frac{[J_f^+(k) - J_f^-(k)]}{\Delta\epsilon} - \frac{[J_{el}^+(k) - J_{el}^-(k)]}{\Delta\epsilon} \\ & + \sum_{s,j} N_s (R_{sjk+m_{sj}} + R'_{sjk-m_{sj}} n_{k-m_{sj}} N_s^j / N_s + R_{sk+m_{si}}^i n_{k+m_{si}} \\ & + \delta_{1k} \sum_m R_{sm}^i n_m - (R_{sjk} + R'_{sjk} + R_{sk}^i) n_k) \end{aligned}$$

with

$$\begin{aligned} J_f^+(k) &= \frac{2Ne^2}{3m} \left(\frac{E}{N} \right)^2 \frac{\epsilon_k^+}{v_k^+ / N} \left(\frac{n_{k+1} + n_k}{4\epsilon_k^+} - \frac{n_{k+1} - n_k}{\Delta\epsilon} \right) , \\ J_{el}^+(k) &= v_k^+ \left[\frac{n_{k+1} + n_k}{2} \left(\frac{kT}{2} - \epsilon_k^+ \right) - kT\epsilon_k^+ \left(\frac{n_{k+1} - n_k}{\Delta\epsilon} \right) \right] \end{aligned}$$

and

$$\begin{aligned} \frac{v_k^+}{N} &= \left(\frac{2\epsilon_k^+}{m} \right)^{1/2} \sum_s q_s \sigma_s(\epsilon_k^+) , \\ \bar{v}_k^+ &= 2mN \left(\frac{2\epsilon_k^+}{m} \right)^{1/2} \sum_s \frac{q_s \sigma_s(\epsilon_k^+)}{M_s} , \end{aligned}$$

where

$$\epsilon_k^+ = k\Delta\epsilon, \quad \epsilon_k^- = \epsilon_{k-1}^+,$$

$$J^-(k) = J^+(k-1), \quad m_{sj} = \epsilon_{sj}^*/\Delta\epsilon$$

The complete code is maintained by Captain (Major Selectee) Hunter of the Physics Department at AFIT.

VITA

William R. Ercoline was born on 26 October 1945 in Charleroi, PA. He is the son of Mr. and the late Mrs. William Ercoline of Charleroi, PA. He graduated from Charleroi Area Senior High School, Charleroi, PA in 1963. He graduated from California State College (PA) in 1967. He was an instructor pilot in the T-38 aircraft at Randolph AFB, TX until June 1976 when he entered the Air Force Institute of Technology.

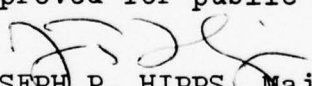
Permanent Address: 517 Conrad Ave.

N. Charleroi, PA. 15022

This thesis was typed by Mrs. Sharon Maruna.

UNCLASSIFIED

SECURITY CLASSIFICATION OF THIS PAGE (When Data Entered)

REPORT DOCUMENTATION PAGE		READ INSTRUCTIONS BEFORE COMPLETING FORM
1. REPORT NUMBER AFIT/GEP/PH/78D-2	2. GOVT ACCESSION NO.	3. RECIPIENT'S CATALOG NUMBER
4. TITLE (and Subtitle) TEMPORAL EVOLUTION OF THE MERCURY-CHLORIDE DISCHARGE		5. TYPE OF REPORT & PERIOD COVERED MS Thesis
		6. PERFORMING ORG. REPORT NUMBER
7. AUTHOR(s) William R. Ercoline Captain, USAF		8. CONTRACT OR GRANT NUMBER(s)
9. PERFORMING ORGANIZATION NAME AND ADDRESS Air Force Institute of Technology (AFIT-EN) Wright-Patterson AFB, Ohio 45433		10. PROGRAM ELEMENT, PROJECT, TASK AREA & WORK UNIT NUMBERS
11. CONTROLLING OFFICE NAME AND ADDRESS Defense Advanced Research Projects Agency Washington DC		12. REPORT DATE December 1978
		13. NUMBER OF PAGES 88
14. MONITORING AGENCY NAME & ADDRESS (if different from Controlling Office)		15. SECURITY CLASS. (of this report) Unclassified
		15a. DECLASSIFICATION/DOWNGRADING SCHEDULE
16. DISTRIBUTION STATEMENT (of this Report) Approved for public release; distribution unlimited		
17. DISTRIBUTION STATEMENT (of the abstract entered in Block 20, if different from Report)		
18. SUPPLEMENTARY NOTES Approved for public release; IAW AFR 190-17 <div style="text-align: center;">  JOSEPH P. HIPPS, Major, USAF Director of Information </div> <div style="text-align: right; margin-right: 50px;"> 19 Jan 79 </div>		
19. KEY WORDS (Continue on reverse side if necessary and identify by block number) Mercury-Chloride Reaction-Rate Constants Temporal Evolution Mercury Cross Section		
20. ABSTRACT (Continue on reverse side if necessary and identify by block number) Computational simulations of the HgCl discharge are discussed. Equations that model the laser are solved simultaneously as functions of time. The discharge model includes electron losses by dissociative attachment and dissociative recombination. Electron sources are direct electron beam ionization and ionization from the excitation of the atomic species. The excitation and ionization rates are obtained from solutions to the electron Boltzmann equation which includes the following processes:		

DD FORM 1473 1 JAN 73 EDITION OF 1 NOV 65 IS OBSOLETE

UNCLASSIFIED

SECURITY CLASSIFICATION OF THIS PAGE (When Data Entered)

UNCLASSIFIED

SECURITY CLASSIFICATION OF THIS PAGE (When Data Entered)

▼
inelastic collisions of the first and second kind, heating by the electric field, secondary electron production by the electron beam, and electron-electron collisions. ←

The HgCl discharge model determines two conclusions. First, the significant metastable levels of Mercury for determining the reaction rate constants are the $6^3P_{0,1,2}$ and 6^1P_1 levels. Second, that the discharge is highly sensitive to the concentration of chlorine.

UNCLASSIFIED

SECURITY CLASSIFICATION OF THIS PAGE (When Data Entered)

